SERI/STR-211-2932
UC Category: 63
DE86010699

MASTER

An AlGaAs-GaAs Patterned Ge Tunnel Junction Cascade Concentrator Solar Cell

Annual Subcontract Report
15 October 1984 - 14 October 1985

Research Triangle Institute
Research Triangle Park, NC

SERI/STR--211-2932

DE86 010699

May 1986

SERI Technical Monitor:
R. Mitchell

Prepared under Subcontract No. XL-4-03032-6

Solar Energy Research Institute
A Division of Midwest Research Institute

1617 Cole Boulevard
Golden, Colorado 80401-3393

Prepared for the
U.S. Department of Energy
Contract No. DE-AC02-83CH10093

EB

TABLE OF CONTENTS

Page

LIST OF FIGURES

1.0 INTRODUCTION

1.1 Background

A major goal of the National Photovoltaics Program is to demonstrate a power conversion efficiency of 30 percent for a small-area, multi-junction solar cell. A variety of semiconductor materials and approaches have been proposed and partially developed to achieve this goal. The materials include the group IV and several group III-V compound semiconductors. The approaches range from a 4-terminal, mechanically-stacked configuration containing two separately optimized individual cells to a 2-terminal, fully-monolithic integration of two photovoltaic p-n junctions.

Monolithic growth of two photovoltaic junctions of different energy bandgaps and possessing the same polarity creates a third intermediate junction of opposite polarity. This third junction must be fabricated such that it does not generate a photovoltage and does not present a high-value resistance in electrical series with the 2 photovoltaic junctions. In addition, this third junction needs to be transparent to the light transmitted through the wide bandgap top cell to the narrower bandgap bottom cell to minimize optical losses.

One attractive approach to the monolithic cascade cell is the AlGaAs/GaAs system in which the top cell is $Al_{.38}Ga_{.62}As$ (Eg = 1.89 eV) and the bottom cell is GaAs (Eg = 1.43 eV). While this approach does not offer the absolute maximum theoretical efficiency, it does offer several attractive features. The structure is nearly perfectly matched in lattice constant and thermal expansion coefficient to the GaAs substrate. A substantial technology base exists for these compound semiconductors, and the potential efficiency for a concentrator cascade cell may exceed 30 percent.

Initial attempts at RTI and at other laboratories to develop the AlGaAs/GaAs monolithic cascade multijunction cell centered upon use of an n^+/p^+ $Al_{.35}Ga_{.65}As$ tunnel junction as the intermediate third junction, or the intercell ohmic connection (IOC). This approach is handicapped by several fundamental and technological problems.

Because of the large bandgap of this tunnel junction ($Eg = 1.86$ eV) and its relatively low maximum attainable n- and p-type doping concentrations, tunnel junctions exhibiting high peak current densities, J_p, have never been demonstrated. The maximum value of J_p obtained for $Al_{.14}Ga_{.86}As$ is 18 A/cm^2; as a reference, the maximum value of J_p reported for GaAs is 40 A/cm^2 [1]. The minimum current density an $Al_{.35}Ga_{.65}As$ planar tunnel junction must conduct, allowing only a small voltage drop ($\sim$ 50 meV) for a 400 sun concentration, is 4 A/cm^2. Typical $Al_{.35}Ga_{.65}As$ n^+/p^+ tunnel junctions exhibit peak current densities much less than 1 A/cm^2.

Another problem is that heavily-doped $Al_xGa_{1-x}As$ alloy layers, particularly the n^+ Te-doped layer, exhibit a fairly rough surface morphology, which tends to reduce the open circuit voltage of the wide bandgap top cell.

1.2 Central Theme

An attractive solution to these problems is to use a patterned tunnel junction that is grown in Ge. This connecting junction is photolithographically defined into the same pattern as the top contact grid and, when the two are properly aligned, will introduce little additional shadowing of the bottom cell. The reduction in the connecting tunnel-junction area should be compensated by the substantially improved conductivity of the heavily-doped Ge layers in comparison with the higher bandgap AlGaAs tunnel junction in conventional planar structures.

The patterned tunnel-junction structure offers several important advantages related to solving problems presently impeding development of current AlGaAs-GaAs cascade structures utilizing a planar tunnel junction. Because the patterned tunnel junction covers only a small fraction of the bottom-cell area ($\sim$ 5 percent), a substantial portion of the top cell will be grown directly on top of the bottom cell without the intermediate n^+ Te-doped AlGaAs tunnel junction layer. In addition, the patterned structure allows use of a Ge tunnel junction which no longer must be transparent to light incident on the bottom cell. The Ge tunnel junction is expected to yield a substantially reduced tunnel-junction resistance due to its bandgap being lower in energy than the AlGaAs tunnel junction and its larger possible doping concentration. Also. the mismatch of lattice constants and thermal expansion coefficients between Ge and GaAs (0.8 and 1.7 percent, respectively) are less than those between AlAs and GaAs (0.13 and 10.9 percent, respectively).

For 400 to 1000 sun, AM1.5 insolation, and a 5 percent cell coverage, the tunnel junction must be capable of conducting current densities between 100 and 250 A/cm^2 with a voltage drop less than 50 mV. A Ge tunnel junction which conducts up to 16,000 A/cm^2 with a voltage drop of 125 mV has been demonstrated.

Growth of Ge in the OM-VPE reactor is accomplished by pyrolytic decomposition of GeH_4 in a manner identical to epitaxial growth of Si. In addition, both n-type dopants (As) and p-type dopants (B), used successfully to fabricate high current density Ge tunnel diodes, are readily available in the OM-VPE reactor.

1.3 Key Technical Issues

The key technical issues in this approach center on growth and fabrication of a low-resistance Ge patterned tunnel junction (PTJ), and successful overgrowth of a high-efficiency $Al_{.38}Ga_{.62}As$ top cell. For a solar concentration of 1000 suns AM1.5 and a tunnel junction active area coverage of 5 percent, the maximum specific resistance of the complete PTJ interface must be less than $2 \times 10^{-4}\ \Omega\text{–cm}^2$ to provide a tunnel junction voltage drop less than 50 mV. In addition, the OM-VPE growth technology must be capable of growing high-quality $Al_xGa_{1-x}As$ over $Al_yGa_{1-y}As$ previously exposed to wet-chemical processes and ambient air.

1.4 Program Goal and Objectives

The eventual goal of this program is to demonstrate a two-junction cascade solar cell (0.5 cm^2 in area) in the AlGaAs-GaAs material system that has an AM2, 400-1000 sun, power conversion efficiency in excess of 30 percent at a cell temperature of 50°C. This goal will be approached through the accomplishment of several objectives. The objectives for the second year include:

(1) Choice of suitable n- and p-type dopants for the GaAs and $Al_xGa_{1-x}As$ growths.

(2) Growth of heavily degenerated B-doped p^+-Ge epi-layers

(3) Fabrication of intercell ohmic connections (IOC) using n^+–GaAs/p^+–Ge/p^+–GaAs sandwiched structures.

(4) Improvement of GaAs bottom cells and $Al_xGa_{1-x}As$ top cells.

(5) Fabrication of $Al_xGa_{1-x}As$/GaAs cascade solar cell using the patterned n^+–GaAs/p^+–Ge/p^+–GaAs sandwiched structures.

(6) Fabrication of triangular top contacts.

1.5 Accomplishments

The accomplishments obtained in the second year of this program are summarized in this section according to the objective or task listed above.

(1) **Choice of suitable n- and p-type dopants for the GaAs and $Al_xGa_{1-x}As$ growths:**

Si has been qualified to be the best n-type dopant among those evaluated, S, Te, and Si. Mg is the choice for p-type doping although a significant memory effect problem has been clearly identified.

(2) **Growth of heavily degenerate B-doped** p^+-Ge **epilayers:**

B-doped, p^+-Ge growths have been performed. Samples with mirror-like surface morphologies and hole concentrations above 10^{20} cm^{-3} have been achieved.

(3) **Fabrication of intercell ohmic connections (IOC) using** n^+-GaAs/p^+-Ge/p^+-GaAs **sandwiched structures:**

The lowest specific resistance achieved for the n^+-GaAs/p^+-Ge/p^+-GaAs sandwiched IOC is less than 1×10^{-4} ohm–cm^2. However, nonreproducible results have occurred. The cause of this behavior has been identified to be a thin n^+-Ge deposited on the GaAs substrate before the B_2H_6 and GeH_4 flows are established. To solve this problem, a "double doping" method has been adopted; both B_2H_6 and AsH_3 flows are established as the susceptor is brought up to the growth temperature and both are maintained during the growth. Reproducible results for low specific resistivity IOC have been achieved.

(4) **Improvement of GaAs bottom cells and $Al_xGa_{1-x}As$ top cells:**

GaAs bottom cell growths with mirror-like surface morphologies have been routinely obtained. Efficiencies between 8-12 percent at 1-AMO sun have been common even with non-optimized layer thicknesses and a lack of good control of the Mg dopant. For $Al_xGa_{1-x}As$ top cell growths, samples with mirror-like surface morphologies have also been routinely obtained. However, no satisfactory photovoltaic action has yet been measured. This is believed to be due to a lack of moisture removal on the AsH_3 gas line, low growth temperatures, and a lack of optimum control of the Mg dopant.

(5) **Fabrication of $Al_xGa_{1-x}As/GaAs$ cascade cell:**

A complete $Al_xGa_{1-x}As/GaAs$ cascade cell using the patterned n^+-GaAs/p^+-Ge/p^+-GaAs sandwiched IOC has been fabricated. An unambiguous demonstration of voltage addition, and a double breakdown characteristic under illumination have been achieved.

(6) **Fabrication of triangular top contacts:**

A solution containing $20\ H_2O : 20\ H_2O_2 : NH_4OH$ has been identified as an anisotropic etchant for GaAs. However, to achieve a high base angle (>45 °), a dry reactive-ion etch process is suggested.

2.0 DEVICE STRUCTURE

A schematic diagram of a cross section of the patterned tunnel junction cascade solar cell is shown in Figure 2.1. The cross section is taken through one set of aligned patterned-tunnel-junction and top-contact grid stripes. Approximate choices for the alloy composition, impurity concentration, and thickness of each of the layers are shown in Figure 2.2, and a schematic energy-band diagram for the structure is shown in Figure 2.3.

The 1.89 eV bandgap of the base n-type region of the top cell is chosen to provide a current match between the top and bottom cells for AM1.5 insolation.

The graded-bandgap p-type surface layers for both top and bottom cells serve four separate functions. Two of these functions are unique to graded-bandgap cells, and two are similar to heteroface cells with constant-bandgap surface layers. The two functions unique to GBG cells are to increase the photogenerated current collected from these regions and the photovoltage generated by each cell. Both of these effects result from the presence of a quasi-electric field acting upon the minority carriers. As discussed below, each of these contributions is modest, being 2.5-3 percent each for current and voltage. However, optimization of the device structure may increase the combined improvement of current and voltage up to ~ 7 percent. This is an appreciable gain in efficiency, considering that growth of the graded-bandgap regions is compatible with OM-VPE growth of the required layers and with the need for window layers for each of the cells. The other two functions required of the

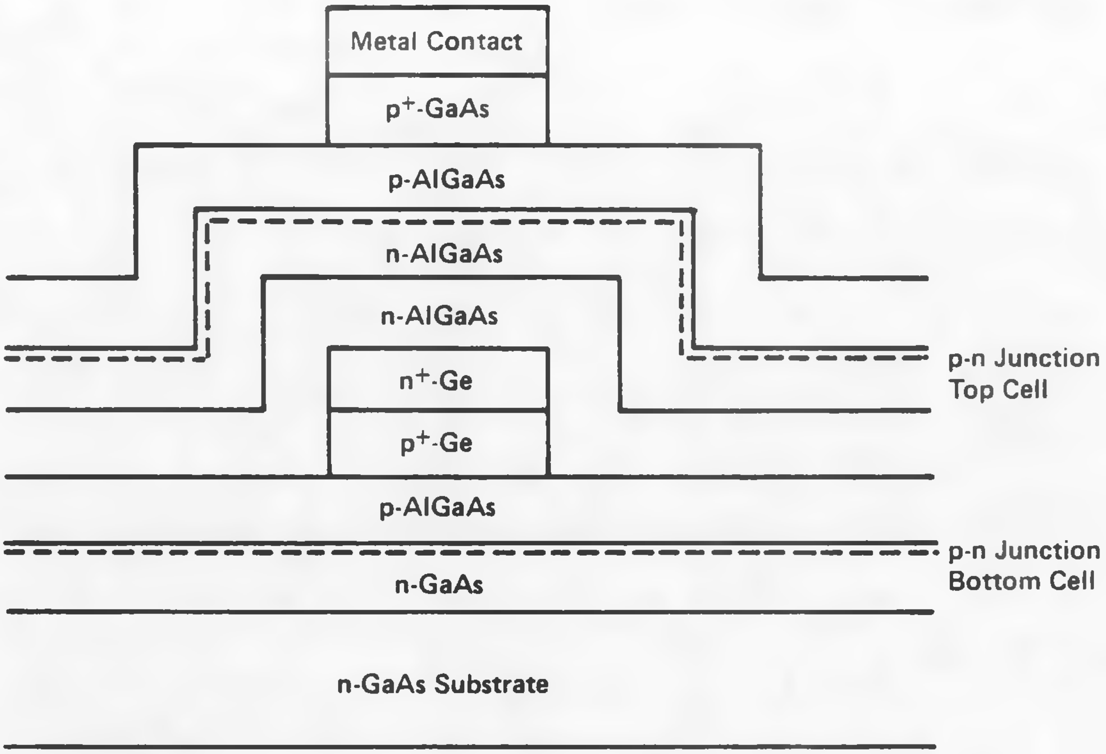

Figure 2.1 Structural diagram of the graded-bandgap AlGaAs-GaAs patterned-tunnel-junction cascade solar cell.

Layer	$n(cm^{-3})$	$p(cm^{-3})$	Thickness (μm)	AlAs (%)
p-GaAs		5×10^{18} (Mg)	1.7	0
p-$Al_xGa_{1-x}As$		1×10^{18} (Mg)	0.5-1	$0.38 < x < 0.45$
n-$Al_xGa_{1-x}As$	1×10^{18} (Si)		3	0.38
n-$Al_xGa_{1-x}As$	1×10^{18} (Si)		0.15	0.92
n^+-Ge	5×10^{19} (As)		0.15	0
p^+-Ge		5×10^{19} (B)	0.15	0
p-$Al_xGa_{1-x}As$		1×10^{18} (Mg)	0.5-1	$0 < x < 0.45$
n-GaAs	1×10^{18} (Si)		4	0
n-GaAs	2×10^{18} (Si)		Substrate	0

Figure 2.2. Detailed doping and thickness data for structure shown in Figure 2.1.

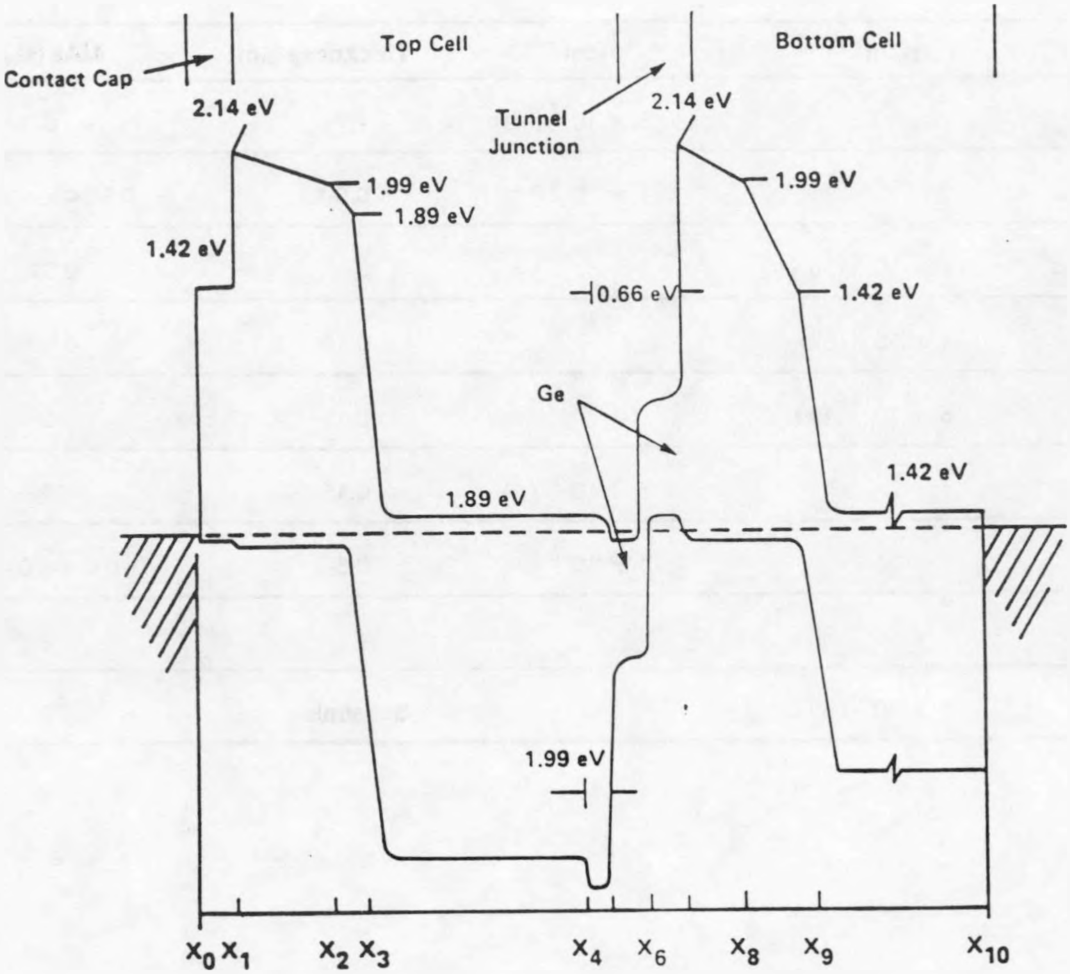

Figure 2.3. Energy band diagram of AlGaAs-GaAs graded bandgap Ge-patterned-tunnel-junction cascade solar cell.

surface graded-bandgap layers are to provide a minority-carrier energy barrier. to prevent back-diffusion of photogenerated electrons, and to provide a low-resistance path for the lateral flow of current to a contact (top cell) or tunnel-junction (bottom cell) stripe. The first two functions require thin graded-surface layers to maximize the quasi-electric field, and relatively low acceptor concentrations $\sim$1–5 $\times$ 10^{17} cm^{-3}. However, the last function requires just the opposite, or thick layers and high acceptor concentrations.

The $Al_{.45}Ga_{.55}As$ layer between X_4 and X_5 in Figure 2.3 is required to place an energy barrier for photogenerated holes between the n-type base region of the top cell and the tunnel junction, which will prevent undesirable diffusion of these holes into the p-type emitter layer of the bottom cell. This barrier could also be generated by grading the base region of the top cell between X_3 and X_4. While this would serve to further increase the open-circuit voltage of the top cell and the hole collection efficiency of the base region, it would also increase the optical transmission of the top cell. This increased transmission would then cause additional absorption and current generation in the bottom cell, and thereby destroy the current match between cells. Similar electron diffusion barriers are provided for the surface regions of each cell by the graded bandgap $Al_xGa_{1-x}As$.

A central feature of the structure is the patterned Ge tunnel junction (PTJ) which should provide a very low-resistance interconnect between the top and bottom cells. Also, because it is hidden under the top metalization, the Ge PTJ should offer very little obscuration to light transmitted by the top cell.

A Ge IOC which covers 5 percent of the cell area must have a specific resistance less than 2×10^{-4}ohm - cm^2 to restrict a deleterious voltage drop to less than 50 mV at 250 A/cm^2 for 1000-sun, AM1.5 concentration. The Ge IOC consisting of sandwiched n^+–GaAs/n^+–Ge/p^+–Ge/p^+–GaAs growth, however, has presented some difficult problems, such as diffused junction, and non-degenerate n^+-Ge layer growth. Work conducted during this second year clearly shows the minimization of the specific resistance using the n^+–GaAs/p^+–Ge/p^+–GaAs sandwiched structures. This is a significant result because it simplifies the Ge growth and avoids the problem of As diffusion. The experimental results are presented in the next three sections.

3.0 DOPING STUDIES IN GaAs AND AlGaAs

To grow solar cell devices with good characteristics, it is necessary to have an accurate control of the doping and interfaces and to be able to grow highly doped layers. Diethyltellrium (DET) (105 ppm in H_2), hydrogen sulfide (H_2S) (5 ppm in H_2) and silane (40 ppm in H_2) have been used for n-type doping studies in GaAs. Dimethylzinc (DMZ) (90 ppm in H_2), bis(cyclopentadienyl)magnesium (Cp_2Mg) and bis(methylcyclopentadienyl) magnesium (MCpMg) have been used for p-type doping studies. A growth temperature of 650°C has been used in these studies since one program objective is to grow cascade cells below 700°C. Samples were exposed to a single dopant at a time. However, within a single growth, dopant flows were varied to produce multilevel carrier concentrations, to examine diffusion properties, and to identify system memory effects. Polaron electrochemical profiling was used to measure the carrier concentrations versus epitaxy depth. The results are described in the next section.

3.1 N-type Doping

Tellurium is the first n-type dopant considered. Figure 3.1 shows the intended and actual doping profile of a typical Te-doped GaAs sample. Carrier concentrations range from the low- to mid-10^{18} cm^{-3}. The actual doping profile failed to follow the intended profile and higher carrier concentrations were obtained for the actual doping profile compared to the intended doping profile. The discrepancy between these two doping profiles is not completely

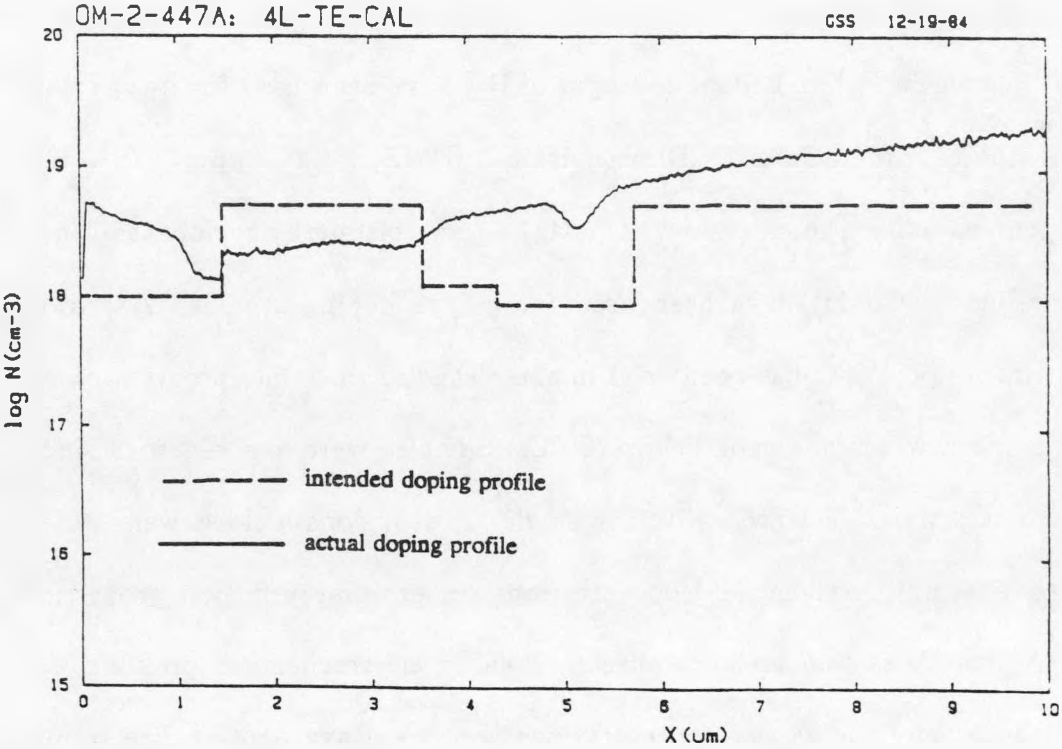

Figure 3.1 Four-layer tellurium-doped GaAs calibration study.

understood but may be the result of the memory effect of DET. In general. good doping control was not achieved with DET.

For the H_2S source, the carrier concentrations range from the low–10^{16} to the low–10^{17} cm^{-3} and suggest a more concentrated source is needed for the base region of the bottom cell. In addition, significant diffusion is indicated by the Polaron profile in Figure 3.2. Several lines (A, B, C) with different slopes are associated with the different diffusion times. The interface between layers I and II was heated the longest and shows the greatest amount of diffusion. Lines B and C show smaller and smaller amounts of diffusion as indicated by Θ_2 and Θ_3 being more nearly parallel to the epi-layer surface. No memory effect is indicated in the transition from region III to region IV.

For Si-doped samples, carrier concentrations ranging from low–10^{17} to high–10^{18} cm^{-3} have been achieved. From the Polaron profile shown in Figure 3.3, abrupt junctions are observed and no significant diffusion is indicated. Also, no memory effect has been detected. This behavior agrees with observations of Azoulay et. al. [2]. Thus, SiH_4 has been selected as the n-type GaAs dopant. For the same reasons, SiH_4 will be used as the n-type dopant for $Al_xGa_{1-x}As$ growth. For Si-doped $Al_xGa_{1-x}As$ ($x = 0.25$) at 750 °C, doping levels of 10^{18} cm^{-3} with mirror-like surface morphologies have been achieved.

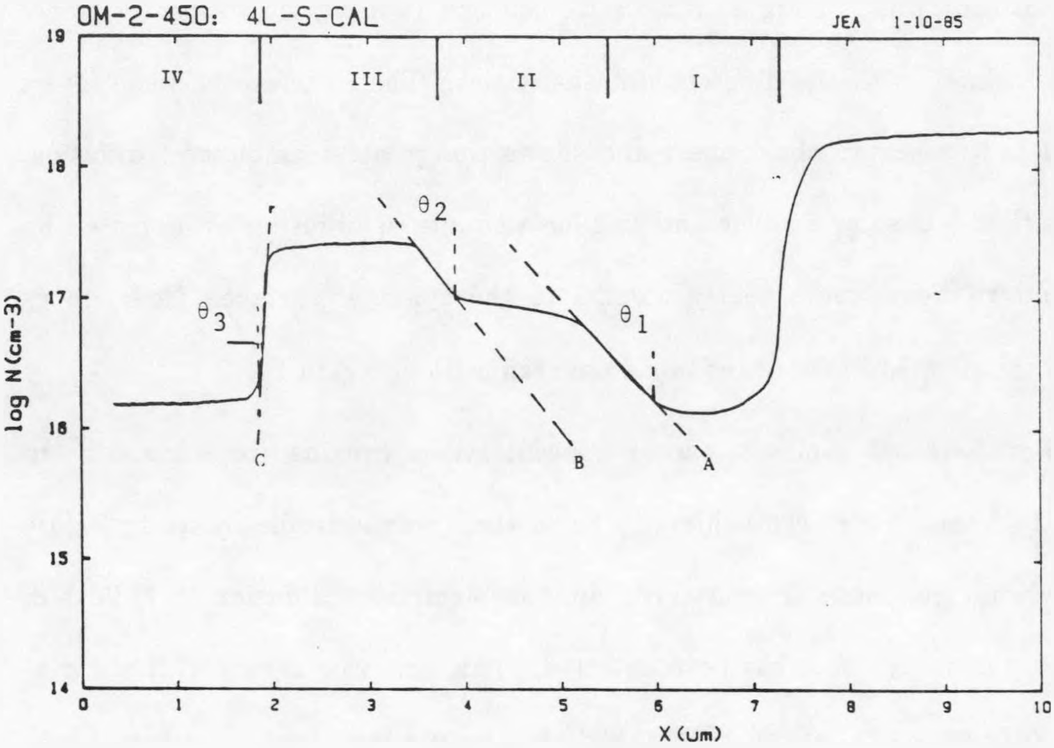

Figure 3.2. Four-layer sulfide-doped GaAs calibration study.

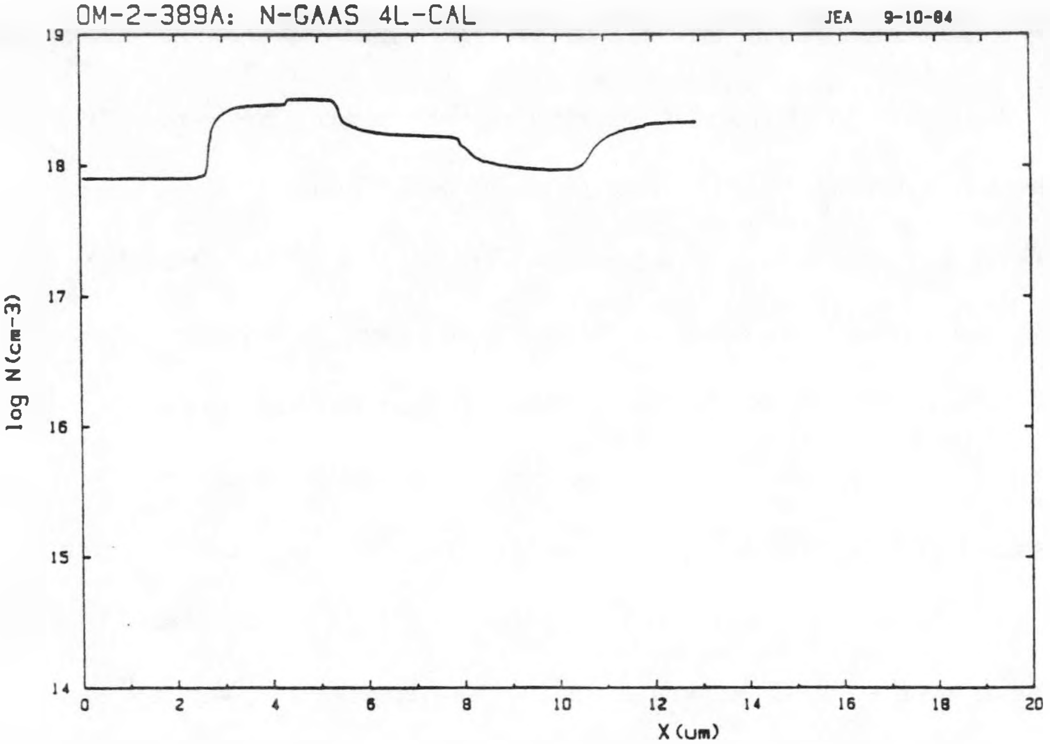

Figure 3.3. Four-layer silicon-doped GaAs calibration study.

3.2 P-type Doping

One difficult problem encountered during the course of this program has been the development of suitable p-type doping for GaAs and AlGaAs. Carrier concentrations above the low–10^{17} cm^{-3} range have not been obtained in work using the dilute DMZ source. Too, the Polaron plot of Figure 3.4 indicates significant diffusion, expected behavior for Zn at 650°C.

Magnesium (Mg) provides the most realistic alternative because it is less toxic than berylluim (Be) and less diffussive than zinc (Zn) on cadmium (Cd). However, Mg sources present a problem. This doping problem manifests itself by an "all or nothing" effect in which grown layers show either high carrier concentration ($\geq 10^{19}$ cm^{-3}) and very poor surface morphologies or they have poorly controlled, compensated carrier concentrations (some layers are n-type) but good surface morphologies. This behavior has been observed for two different Mg sources, Cp_2Mg and MCpMg. It was believed initially that the behavior resulted from impurities in the Cp_2Mg and MCpMg; however, we now believe it results from a combination of a substantial "memory" effect in our OM-VPE system and a very narrow doping "window".

The memory effect is produced by absorption of the organometallic source on the stainless tubing walls and, depending upon system configuration, results in lengthy periods before the gas stream above the heated substrate contains an equilibrium concentration of the reactant. The time required to achieve equilibrium depends on the rate with which the Cp_2Mg or MCpMg is

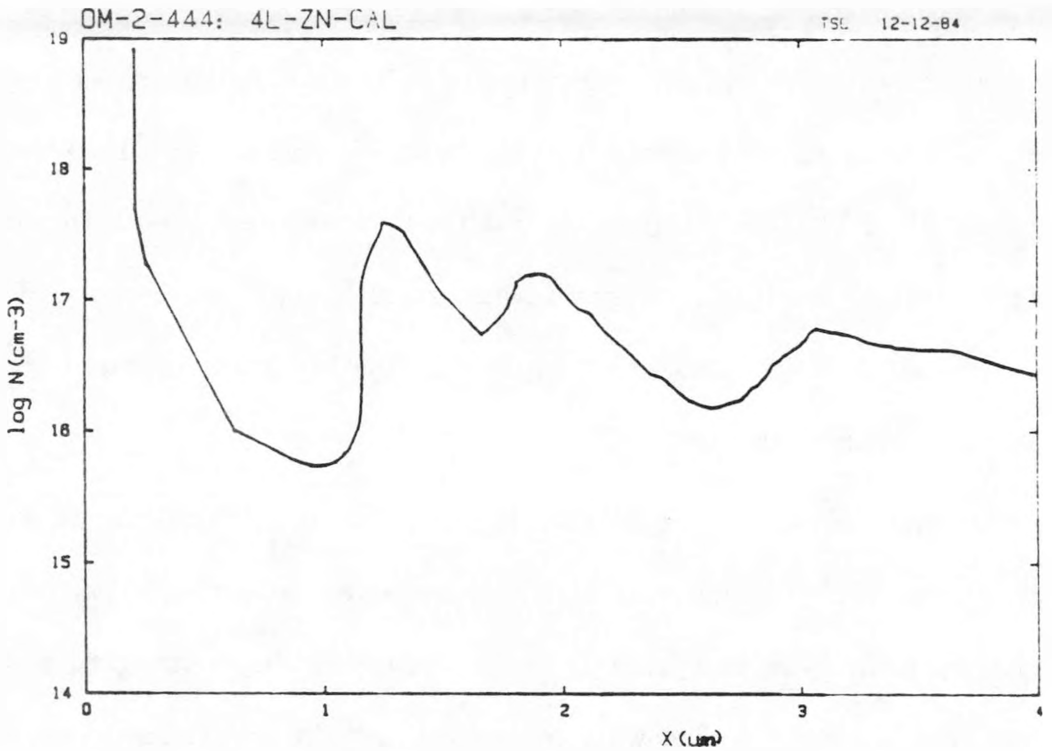

Figure 3.4. Four-layer zinc-doped GaAs calibration study.

transferred from the bubbler and the length of the steel tubing prior to injection into the reactor tube. Once injected into the reactor tube, the high carrier gas flow rates probably limit the lateral diffusion to the quartz walls. Hence, most of the delay is thought to occur in the stainless tubing.

The growth system configuration plays a significant role in the extent of the memory effect. In systems which use the vent-run approach, the lines can be equilibrated before the Mg reactants are switched into the reactor. (This assumes a small volume between switching manifold and reactor tube.) Unfortunately, the RTI OM-VPE system is not thusly configured and a rather long length of tubing must be equilibrated before stable doping can be achieved. A modification to reconfigure our system so that the Mg line is operated in the vent-run mode is underway.

Attempts to rapidly equilibrate the Mg line using high carrier flows through the OM-Mg bubbler and high reactant partial pressures (i.e. high bubbler temperatures) are hampered by the second factor, the narrow doping window. With a narrow doping window small changes in dopant gas phase concentration produce large changes in the solid. Care must be exercised to avoid exceeding the solid solubility limit of Mg in GaAs, as described by Lewis et. al. [3] because of the poor surface morphologies which result. A narrow doping window has also been reported for Cp_2Mg in InP [4].

Experimental evidence supports the memory-effect and doping-window interplay. SIMS and C-V analyses both indicate graded doping. Figure 3.5 shows a SIMS profile of a GaAs sample which was grown for 65 minutes, 60

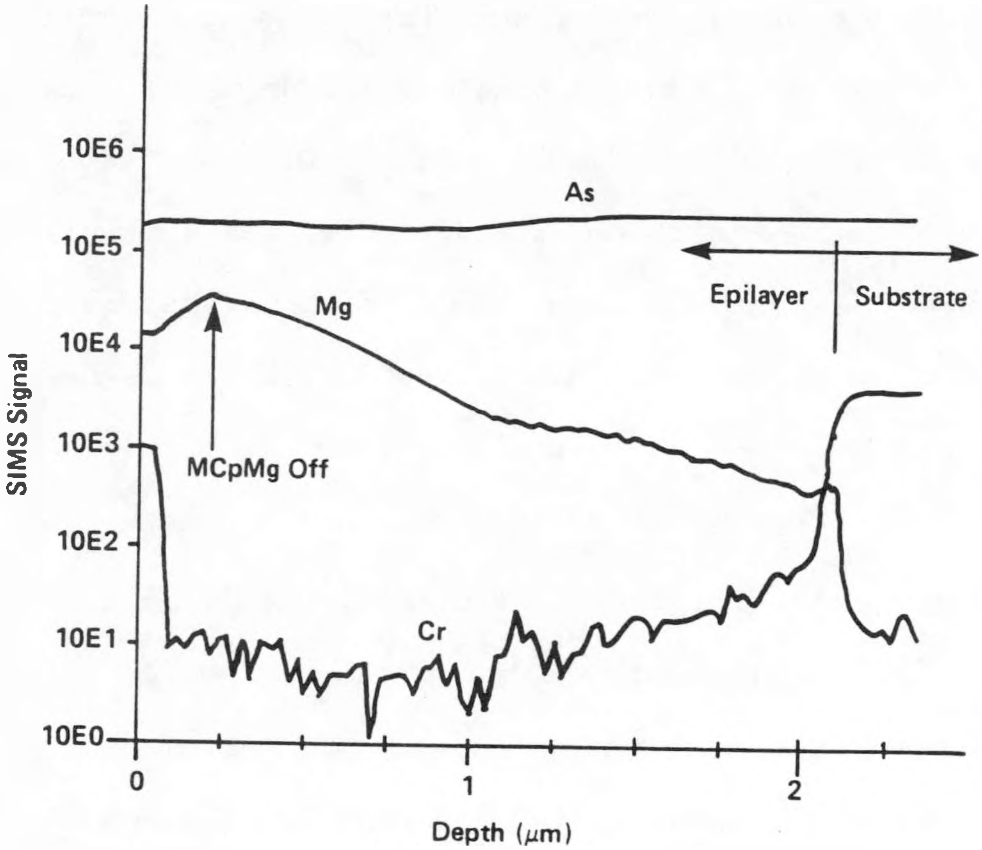

Figure 3.5. Mg profile in 2-μm thick GaAs layer measured by SIMS.

minutes with a MCpMg flow and 5 minutes of additional GaAs growth after the H_2 carrier flow in the MCpMg bubbler was terminated. The layer is approximately 2-μm thick and has an excellent surface morphology. The SIMS data show a monotonic increase in the Mg content of the layer until the Mg flow is stopped. At that point desorption from the tubing walls prevents a rapid drop off in Mg concentration, and the desorption downward slope approximately equals the increasing slope. This suggests the presence of wall effects. At the growth conditions being used, the Mg content in the solid never reaches an equilibrium value and grades approximately an order of magnitude per micrometer of growth. The absence of a reliable standard make quantitative Mg determination impossible, but Hall-effect analysis for this sample indicates an average carrier concentration of 9.9×10^{17} cm^{-3} supported by C-V data which show a carrier grading from less than 2×10^{17} to over 2×10^{18} cm^{-3} before breakdown in the sample.

Photoluminesce (PL) provided a demonstration of the persistence with which MCpMg, and presumable Cp_2Mg, can adhere to the tubing walls. PL (77K) examination of an unintentionally doped $Al_{0.3}Ga_{0.7}As$ layer revealed substantial Mg acceptor emissions. The Mg identification was confirmed from a sample of $Al_{0.3}Ga_{0.7}As$ doped with Mg. The MCpMg source had not been used for two days prior to the growth of this AlGaAs layer, but the sweep air temperature in the OM-VPE cabinet was below the melting point (27 °C) of the MCpMg. Condensed MCpMg on the tubing walls provided the doping source for the subsequent AlGaAs growth. As a result, the Mg line has been heated and maintained at 40 °C to reduce any potential problems. and, indeed, the long-term persistence has not been observed since.

In spite of the doping grading, GaAs layers have been grown with p-type carrier concentration ranging from 1×10^{16} to 2×10^{19} cm^{-3} using MCpMg (average values measured by Hall analysis). These layers have very good surface morphologies until the average concentrations exceed approximately 7 or 8×10^{18} cm^{-3}. At this point the Mg concentration near the surface has likely exceeded the solid solubility limit, and a poor morphology results.

A Mg-doped $Al_xGa_{1-x}As$ layer ($x = 0.3$) has been grown for which a Hall measurement indicates a carrier concentration of 1.1×10^{19} cm^{-3}. This result is significant because the surface morphology is excellent, specular and free surface defects, and is one of the highest carrier concentrations reported for AlGaAs in this composition range.

To summarize, Si has been qualified to be the best n-type dopant among those evaluated, S, Te, and Si. Several factors have been positively identified for Si-doped GaAs. Those factors include:

1. very good control of carrier concentration (from low- 10^{17} to high- 10^{18} cm^{-3}),
2. abrupt interfaces, and
3. no memory effect in the OM-VPE growth system.

In the case of the p-type dopant, both Cp_2Mg and MCpMg have been identified to have a substantial memory effect. This problem. however. can be eased using a vent/run configuration in the growth system. Once the problem is solved, Mg will likely emerge as the most suitable dopant for the p-type layers required in this program.

4.0 DEVELOPMENT OF Ge-RELATED TECHNOLOGIES

This program began with the goal of growing Ge homojunctions showing low resistivities. However, subsequent specific resistivity measurements indicate that a completely adequate IOC can be grown using an n^+-GaAs/p^+-Ge/p^+-GaAs sandwiched structure. This is a significant result because it simplifies the Ge growth and avoids the problem of As diffusion.

In this section, we describe the growth of B-doped p^+Ge and the achievement of low resistivity using this sandwiched structure.

4.1 Growth of Boron-doped Ge

A significant development for p^+-Ge growth has been achieved this year; this development concerns the carrier concentration, growth rate, and surface morphology of the B-doped Ge epilayers and is described below.

The diborane (B_2H_6) source, 1000 ppm B_2H_6 in H_2, has been used in this study. For these experiments, the GaAs substrates were heated to growth temperatures between 570 and 625 °C and stabilized for 5 minutes under an AsH_3 overpressure. Before the B_2H_6 and GeH_4 flows were established, the AsH_3 flow was terminated and followed by a H_2 gas purge for 3 minutes. At the end of the growth interval, the GeH_4 flow was terminated, and the system remained at the growth temperature for an additional 1 minute. The susceptor and substrate were then cooled to 400 °C in the B_2H_6/H_2 ambient, followed by an H_2 purge until the susceptor reached room temperature.

Two significant features for boron (B) doping are: (i) the solid solubility of B in Ge is greater than 10^{20} cm^{-3}, and (ii) B_2H_6 has a high vapor pressure. Thus, B, if not incorporated in the crystal lattice, will desorb from the substrate surface. Using room temperature Hall effect analysis, hole concentrations ranging from 4×10^{19} to 3.5×10^{20} cm^{-3} have been measured. Results are shown in Figure 4.1. There is a considerable increase in the doping level when the growth temperature drops from 625 to 570 °C. This behavior can be explained by reduced desorption rates of B from the surface enhancing the chance of incorporation into the crystal.

For n-type doping in Ge, AsH_3 (10 percent in H_2) serves as the source, and carrier concentrations range from 0.8 to 2×10^{19} cm^{-3} at a growth temperature of 625 °C. Results for AsH_3 doping are also included in Figure 4.1. The insensitivity of the carrier concentration to the AsH_3 flow is explained by the saturation of As incorporation into the Ge epi-layers and a high As background in the reactor at the growth temperature. Increased GeH_4 flow produces faster growth and slightly greater As incorporation. Since the effective density of states in the conduction band of Ge is 1.04×10^{19} cm^{-3} [5], these data show that the material is slightly degenerate. However, the effective density of states in the Ge valence band is 6.0×10^{18} cm^{-3} [5], indicating that all the B-doped, p-type samples are deeply degenerate.

Figure 4.2 shows that the Ge growth rate increase slowly from 0.05 to 0.12 μm/min as the B_2H_6 flow increases from 0 to 300 cm^3/min. The growth rate appears slightly lower at 570 °C than 625 °C which might also contribute

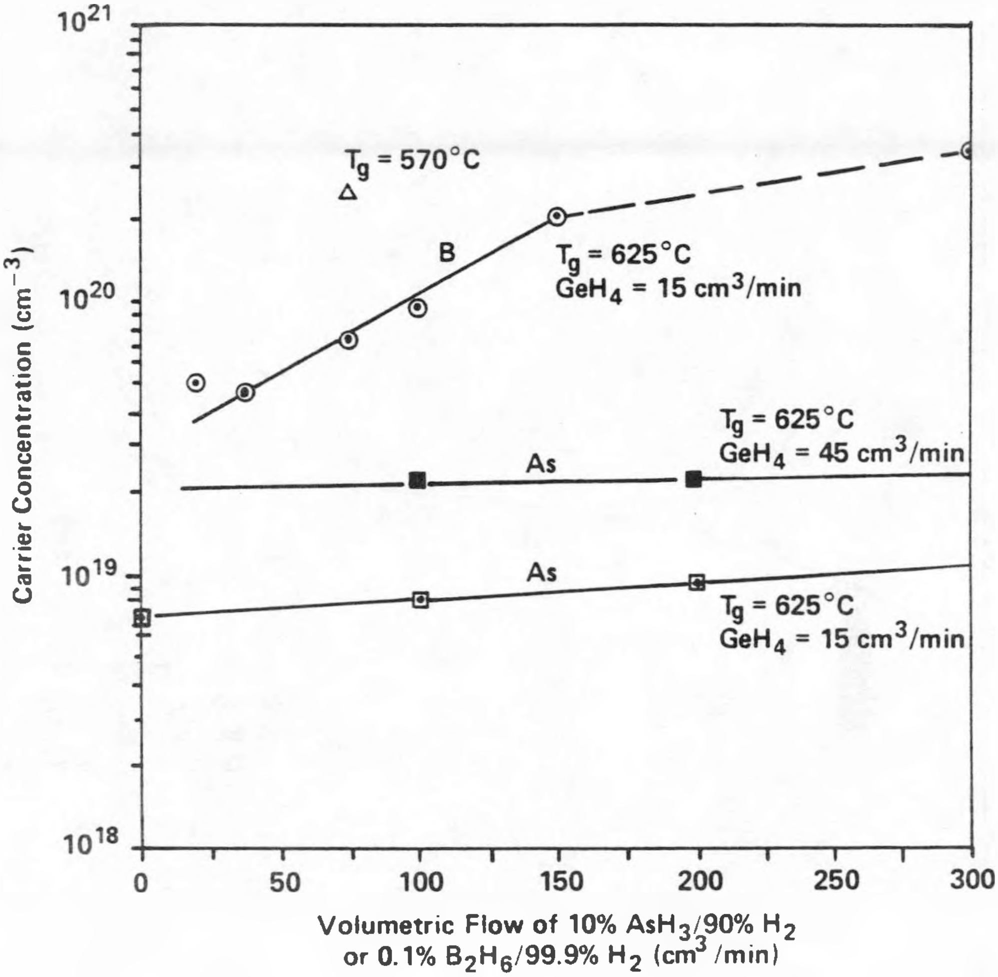

Figure 4.1. Doping characteristics of As and B as a function of AsH_3 and B_2H_6 flows respectively.

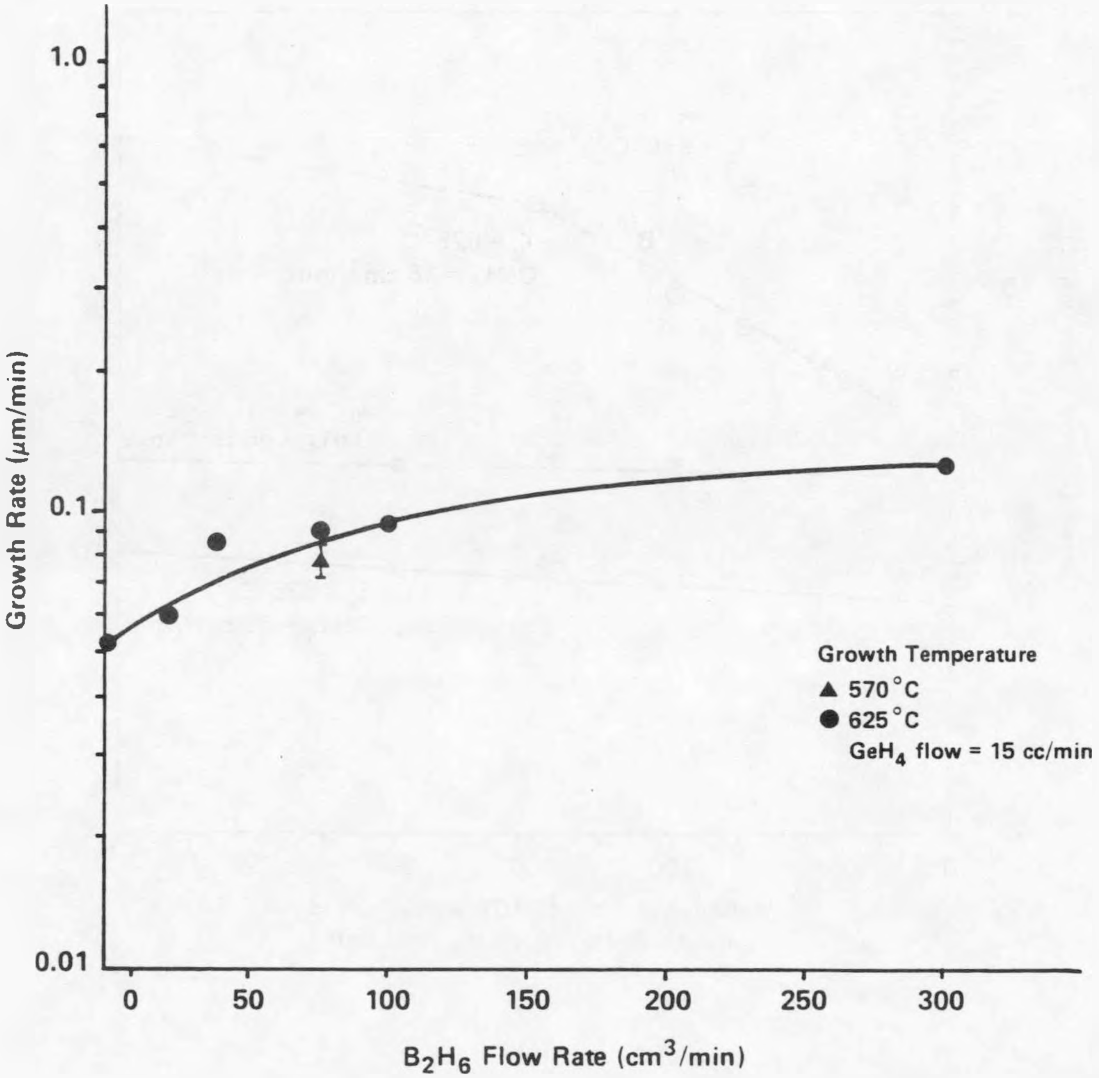

Figure 4.2. Growth rate versus flow rate of B_2H_5 (growth temperature:▲= 570 °C,●= 625 °C, GeH_4 flow= 15 cc/min).

to the increased B concentration at the lower temperature.

Figure 4.3 shows a micrograph of a Ge surface which is mirror-like and defect-free to the naked eye. Microscopic examination reveals a slight orange-peel look. Surface morphologies remain mirror-like for hole concentrations below 2×10^{20} cm^{-3} but degradation above this level occurs as the solid solubility of B in Ge is approached. While some dopant clustering may be present, no problems such as the Ga droplets reported last year have been observed.

Based on these results, we have concluded that B is the optimum p-type dopant for the Ge research in this application.

4.2 n^+–GaAs/p^+–Ge/p^+–GaAs Interconnect Developments

Based on the successful growth of heavily degenerate p^+-Ge layers, efforts have been made to achieve low interface resistivities for n^+–GaAs/p^+–Ge/p^+–GaAs sandwich structures. This structure is attractive because it eliminates one layer of the Ge tunnel junction and uses a heterotunneling interface between Ge and GaAs. The sandwich structures are prepared by growing the p^+–Ge on a p^+–GaAs substrate. A Si-doped GaAs layer (3×10^{18} cm^{-3}) is subsequently grown on the Ge. The structures are processed by applying metal contacts and partially etching the surface. Contact resistance can be measured on unetched areas, and interface resistivity can be approximated from adjacent mesas which have been etched through the Ge-GaAs interfaces into the substrate. (This process is described in last year's Annual Report.)

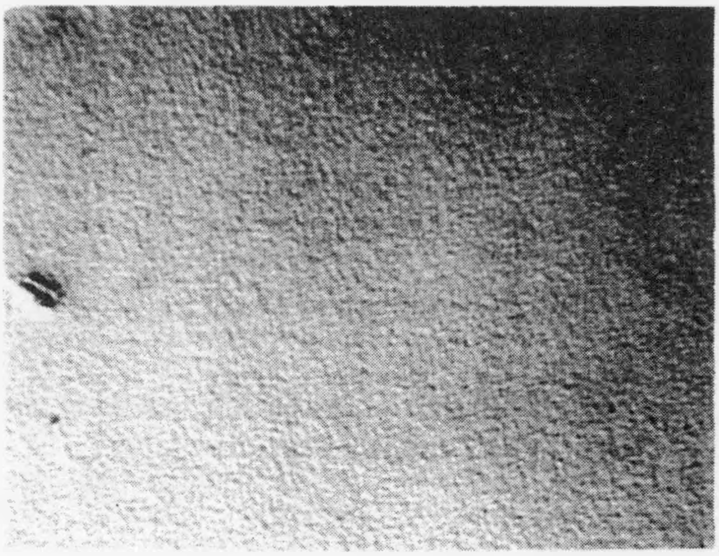

(x710)

Figure 4.3. Surface morphology of a 0.9 μm-thick, B-doped, p^+ - Ge layer deposited on (100) GaAs substrate tilted 2° toward (110). Growth temperature was 625 °C.

In Figure 4.4 the I-V curves are shown for a sandwich structure. The curves in Figure 4.4 (a) were measured between two sets of front surface contact dots. The curves in Figures 4.4 (b) and 4.4 (c) were measured from etched mesa to etched mesa and from the front surface to the back surface, respectively. Subtracting the front contact specific resistivity from the mesa-to-mesa measurement indicates the total n^+–GaAs/p^+–Ge/p^+–GaAs resistivity is less than 1×10^{-4} ohm – cm^2 which meets the program goal for a multicell interconnect operating at 1000, AM1.5 suns (1.7×10^{-4} ohm – cm^2). Both mesa-to-mesa and front-to-back measurements are clearly dominated by the contact resistance.

In the beginning these results have not been reproducible from run to run using the same growth condition. For example, an I-V characteristic from sample OM-480, a p^+-Ge layer grown on a p^+-GaAs substrate, is shown in Figure 4.5, and tunneling behavior is unexpectedly observed. To identify the existing problems, samples have been profiled using secondary ion mass spectrometry (SIMS) recently to determine the doping and the interdiffusion behavior at the interface between p^+-Ge layers and p^+-GaAs substrates. As can be seen in Figure 4.6, the B concentration is one order of magnitude higher than As in the epilayer (region I). Relatively sharp profiles for As and Ge at the interface between the p^+-Ge layer and the p^+-GaAs substrate can be seen in region III. This suggests that diffusion of Ge into GaAs substrates and As into Ge layers might not be a problem. Region II, however, shows that an As-doped, n^+-Ge layer has been deposited on the GaAs substrate before the

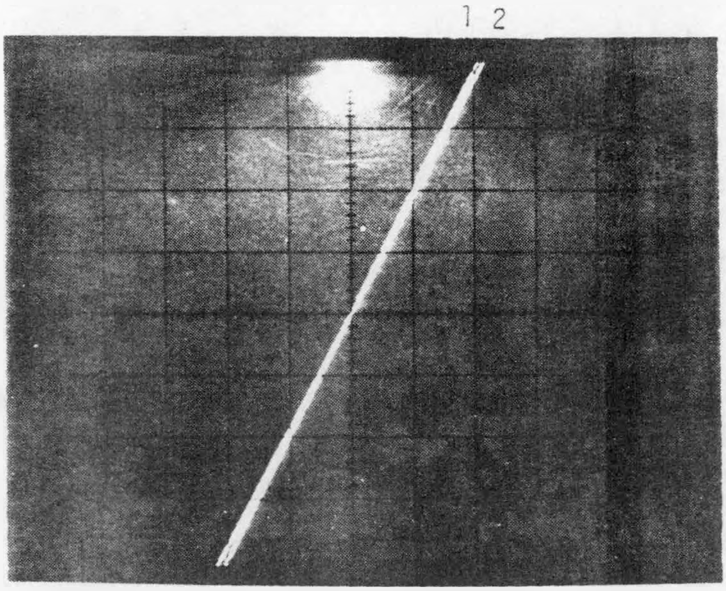

(a)
Ver = 20 mA/div
Hor = 0.1 V/div

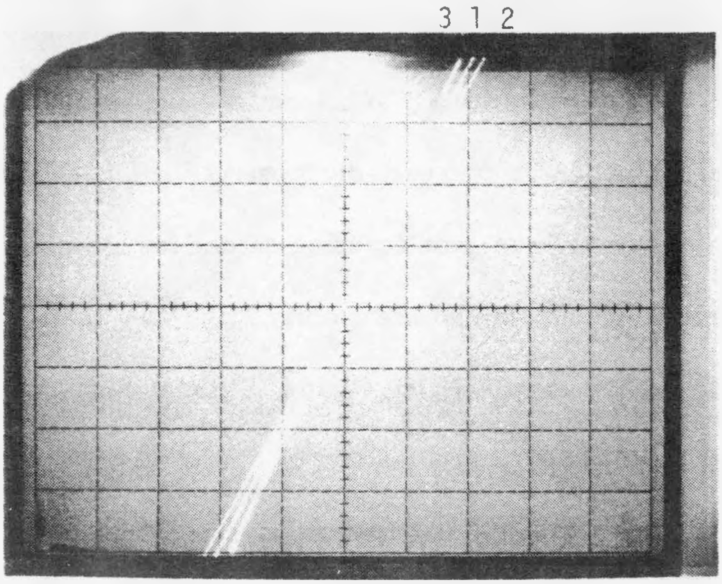

(b)
Ver = 20 mA/div
Hor = 01 V/div

Figure 4.4.(a),(b) I-V characteristic for n$^+$ - GaAs/p$^+$ - Ge/p$^+$-GaAs structure: (a) curves were measured between adjacent contacts on unetched surface, and (b) curves were measured from etched mesa to etched mesa. Curves 1 and 2 were measured on the same contacts as curve 1 and 2 on (a) (growth temperature 625 °C).

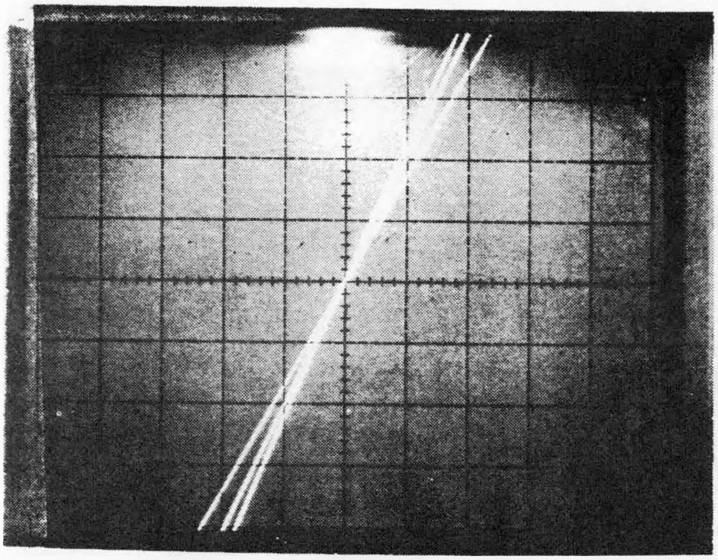

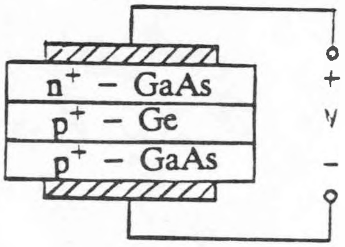

measured structure

(c) Ver = 20 mA/div

Hor = 0.1 V/div

Figure 4.4.(c)I-V characteristic of n^+ - GaAs/p^+ - Ge/p^+GaAs structure (growth temperature 625 ^oC).

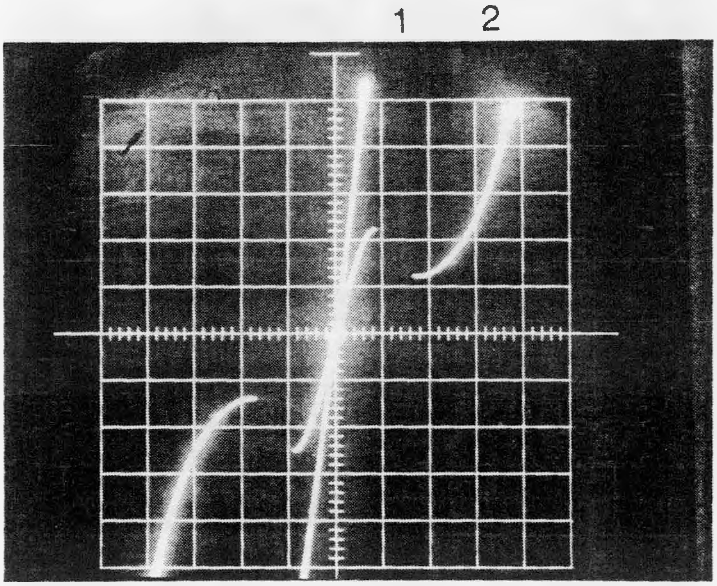

Vertical scale = 5 mA/div
Horizontal scale = 0.1 V/div

Figure 4.5. I-V characteristic for p^+ - Ge/p^+ -GaAs structure. Curve 1 measured between adjacent contacts on unetched surface; curve 2 measured from etched mesa to etched mesa (growth temperature 625 °C).

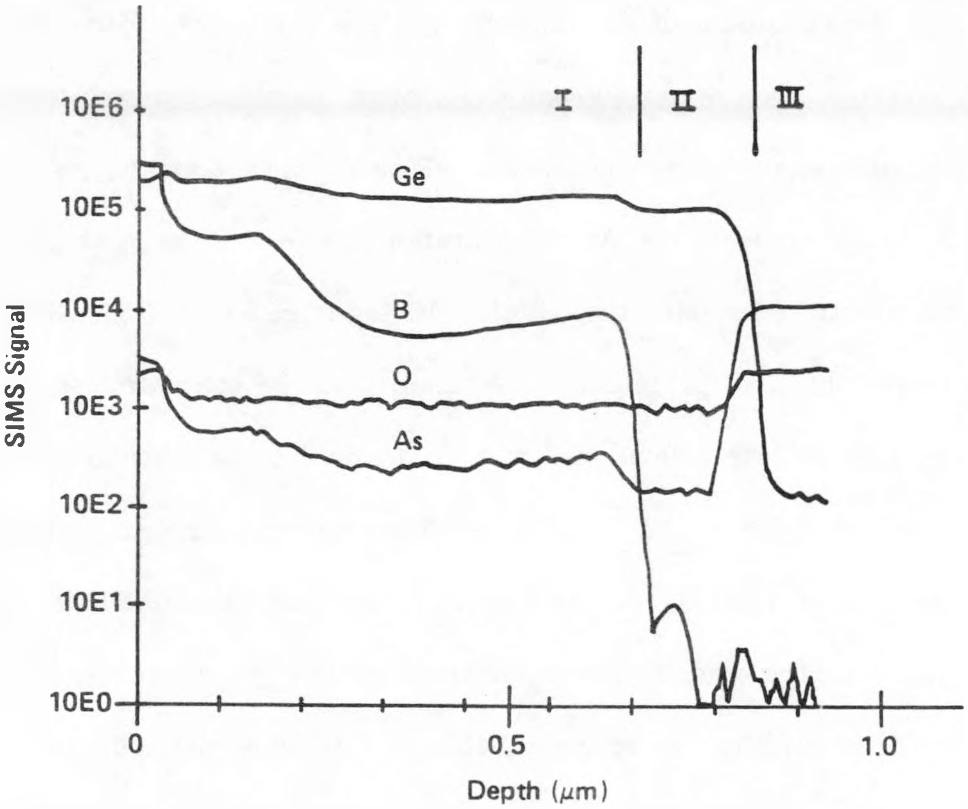

Figure 4.6. SIMS profile in a p^+ - Ge layer grown on p^+ - GaAs substrate (growth temperature 625 °C).

B_2H_6 and GeH_4 flows are established. In this n^+-Ge layer, Ge originates from re-evaporation of deposits on the susceptor from previous growths. As is coming from (i) AsH_3 flow during preheat of GaAs substrate, (ii) decomposition of GaAs substrate, and (iii) wall deposits.

To avoid the deposition of this unwanted n^+-Ge layer, both B_2H_6 and AsH_3 flows are established as the susceptor is brought up to the growth temperature and maintained during the growth. Flowing both dopants, rather than just B_2H_6, also reduces the As concentration gradient between the Ge and the GaAs substrate lessening the diffusion driving force for As from GaAs into the Ge layer. In these "double dopant" samples, carrier concentrations of $|N_A - N_D| \sim 7 \times 10^{19}$ cm^{-3} have been measured. Surface morphologies are mirror-like and defect-free to the naked eye. Microscopic examination reveals slightly cross-hatched patterns (as shown in Figure 4.7), characteristic of growth on (100) surfaces when lattice parameter variation is present. An I-V characteristic demonstrating the success of the double doping method can be seen in Figure 4.8. In this Figure, curve 1 was measured between two front contacts and curve 2 between two mesas etched through the Ge/GaAs interface. Subtracting the front contact specific resistivity from the mesa-to-mesa specific resistivity qualitatively indicates the resistivity at the p^+-Ge/p^+-GaAs interface to be less than 1.7×10^{-4} ohm- cm^2. Data shown in Figure 4.8 are reproducible. Similar data have also been measured for p^+Ge/n^+-GaAs interfaces. This is important because it suggests that a thin, single Ge layer, heavily doped with both B (at $\sim 10^{20}$ cm^{-3}) and As (at $\sim 10^{19}$ cm^{-3}), may

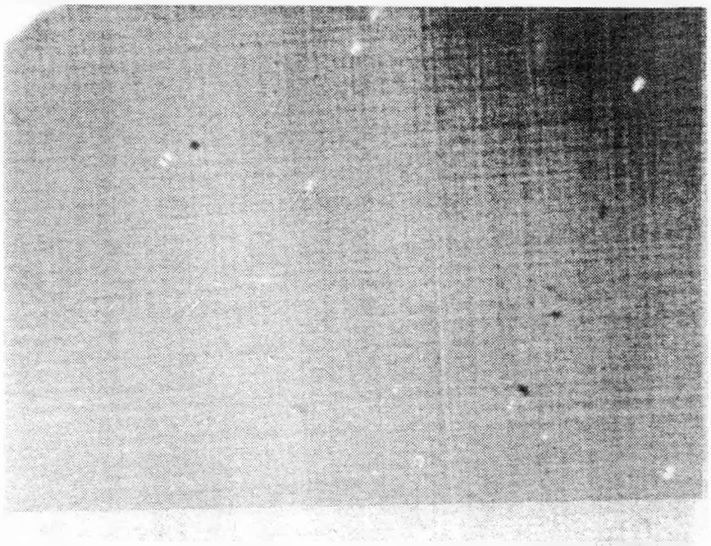

(710

Figure 4.7. Surface morphology of a "double-dopant" Ge sample.

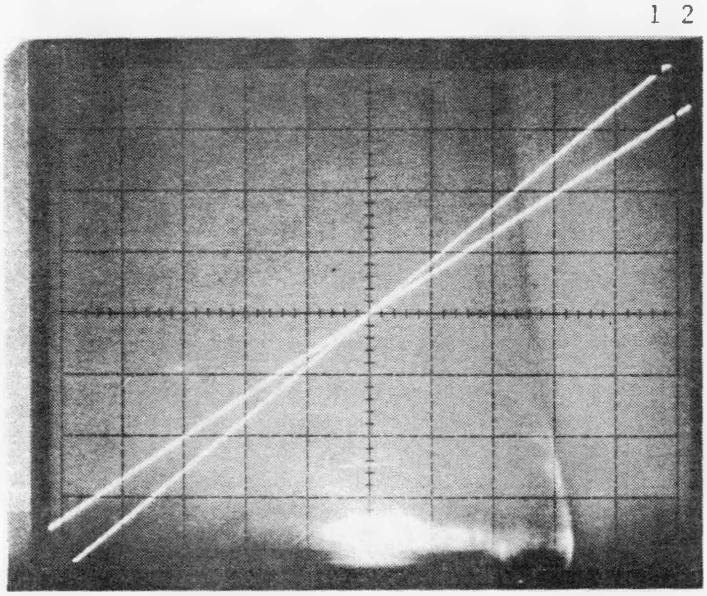

Vertical scale = 50 mA/div
Horizontal scale = 0.05 V/div

Figure 4.8. I-V characteristic for p^+ -Ge/p^+ -GaAs structure. Curve 1 measured between adjacent contacts on unetched surface; curve 2 measured from etched mesa to etched mesa (growth temperature 625 °C).

provide the best and most easily fabricated cascade interconnect yet reported. Initial attempts to connect a top and bottom cell in a cascade structure using the single Ge layer have been made; these attempts appear to be successful and are described in Section 5.3.

4.3 Development of Etching Techniques for Ge Patterned Tunnel Junctions

Since the structures consisting of n^+-GaAs/p^+-Ge/p^+-GaAs with resistivity as low as 1×10^{-4} ohm-cm^2 have been demonstrated, the development of the p^+-Ge etching and the tunnel junction patterning by wet chemical etch have been reinitiated. To our knowledge, a suitable etchant for heavily B-doped p^+Ge has not been reported. Therefore, several etching solutions, as shown in Table 4.1, have been examined.

Initially, we examined a 20 H_2O : 20 H_2O_2 : NH_4OH solution which is frequently used to etch GaAs selectively on $Al_xGa_{1-x}As$ stop etch layers, and has a stable etching rate of 0.3 μm/min for n^+-Ge ($\sim 10^{19}$ cm^{-3}) [6]. For n^--Ge ($\sim 5 \times 10^{15}$ cm^{-3}) etch, we found the etching rate dropped to about 0.12 μm/min. In the case of p^+-Ge ($\sim 9 \times 10^{19}$ cm^{-3}), the etching rate decreases even more strongly to about 0.02 μm/min. Etch rate differentials are as high as 15:1. This is presumably because the B oxides are less soluble than either the Ge or As oxides. Similar behavior for Si has been reported by Kuhn and Rhee [7] who indicate etching rates decrease strongly with increasing B concentration yielding rate differentials as high as 50:1. We have used this solution to pattern n^+-GaAs/p^+-Ge/p^+-GaAs IOCs. However, serious undercutting is always observed. On occasion, the finger patterns have been lost. The slow etching rate for p^+-Ge enhances undercutting during pattern formation.

Other solutions which have been examined are 10 H_2O : HCl : H_2O_2, and 19 NH_4OH : H_2O_2 solutions. Etching rates for both are too low for p^+-Ge and result in serious undercutting during pattern formation.

Higher etching rates can reduce the undercutting problem; thus, we examined solutions containing 95 HNO_3 : 5 HF, and 75 HNO_3 : 25 HF. These solutions, however, etch both p^+-Ge and GaAs layers and leave poor surfaces and have been abandoned for the tunnel junction patterning.

Table 4.1 summarizes the results of the p^+-Ge etching. A suitable wet chemical etchant for either the p^+-Ge or the n^+-GaAs/P^+-Ge/p^+-GaAs structure is still to be identified. If the wet chemical processes do not improve. a selective epitaxial growth of patterned tunnel junction will likely be required to improve cell processing.

Table 4.1. Etching rate for p^+–Ge (N_A–$N_D$$\sim$9 $\times 10^{19}$ cm^{-3})

Etching Solution	Ratio	Etching Rate
H_2O:H_2O_2:NH_4OH	20:20:1	200 Å min^{-1}
H_2O:H_2O_2:HCl	10:1:1	100 Å min^{-1}
H_2O:H_2O_2:HF	4:1:1	1.2 μm min^{-1}
H_2O_2:NH_4OH	19:1	320 Å min^{-1}
HNO_3:HF	95% : 5%	fast, deteriorates GaAs surface
HNO_3:HF	75% : 25%	fast, deteriorates GaAs surface
H_2O:H_2O	10:1	very slow
HF	-	very slow
Buffered HF	-	very slow

To summarize, the growth of B-doped, p^+–Ge epilayers with mirror-like surface morphologies and hole concentrations above 10^{20} cm^{-3} have been achieved. A total interface resistivity of 1.0 $\times$ $10^{-4}\Omega$ –cm^3 has been measured in a structure of n^+–GaAs/p^+–Ge/p^+–GaAs. The problem of reproducibility in resistivity measurement has been identified by SIMS, and a reproducible low specific resistivity connection has been achieved. Etching p^+–Ge is difficult due to a less soluble B oxides, and unless a suitable wet chemical etch technique is developed, selective epitaxial growth of patterned tunnel junction is suggested.

5.0 DEVELOPMENT OF SOLAR CELLS

The development of GaAs bottom cells this year showed encouraging results. Cells with mirror-like surface morphologies have been routinely obtained. Efficiencies between 8-12 percent at 1 AMO sun have been achieved even with non-optimized layer thicknesses and a lack of good control of the Mg dopant.

AlGaAs growth has also improved but still needs considerable development. $Al_xGa_{1-x}As$ top cells with mirror-like surface morphologies have been routinely obtained; however, no satisfactory photovoltaic action has yet been measured. Low growth temperature (700 to 750 °C), lack of moisture removal on the AsH_3 gas line, and lack of optimum control of the Mg dopant are believed responsible for the poor top cell performance.

In the case of cascade cell development, voltage addition has been unambiguously observed. The best cascade cell shows a V_{oc} of 1.44 V at 7 suns (AMO), and the characteristic double breakdown is clearly visible in the I-V curve.

The first step toward fabrication of triangular top contacts has been taken: Preliminary results have identified an anisotropic etch which differentiates between GaAs and $Al_xGa_{1-x}As$ and is suitable for the etching part of triangular contact development.

These results are presented in the following sections.

5.1 P–$Al_xGa_{1-x}As$/p–GaAs/n–GaAs Heterojunction Bottom Cell Development

Bottom cells grown at different temperatures have been fabricated and evaluated. A cell, grown at 650 °C and shown in Figure 5.1, contains an n^+–GaAs buffer layer, an n^+–$Al_{0.3}Ga_{0.7}As$ layer to provide back surface field (BSF), a 2.5-μm-thick, Si-doped GaAs base, a thin Mg-doped GaAs emitter, and a 0.5-μm-thick, Mg-doped $Al_{0.3}Ga_{0.7}As$ window layer. A heavily Mg-doped GaAs layer caps the structure to facilitate contacting. Other cells grown at 700 °C, contain a similar structure except that graded-bandgap, Mg-doped $Al_xGa_{1-x}As$ ($0 \leq x \leq 0.3$) emitters have been included.

Figure 5.2 shows the I-V characteristic of a sample of the first cell type. The open circuit voltages are 0.993 V at 1 AMO sun, and 1.06 V at 8 suns. Fill factors are 0.83 and 0.82 for 1 sun and 8 suns, respectively. The lack of fill factor degradation at 8 suns indicates a good quality contact. The short circuit current, measured without an AR coating, is 17.3 mA/cm^2 at 1 sun. The active area (0.029 cm^2) efficiencies are approximately 10.6 percent and 11.1 percent for 1 sun and 8 suns, respectively. For the second cell type, the open circuit voltages are 0.94 V at 1 AMO sun and 0.991 V at 7 suns, as can be seen in Figure 5.3. Contact resistance for this cell is relatively high and degrades the fill factor to about 0.6. The active area (0.14 cm^2) efficiencies are approximately 8 percent and 6.3 percent for 1 sun and 7 suns, respectively. Thus far, graded emitters have provided no measurable performance advantages.

Cap	p^+–GaAs	0.2 μm
Window	P–$Al_{0.3}Ga_{0.7}As$	0.5 μm
Emitter	P-GaAs	0.2 μm
Base	n - GaAs	2.5 μm
BSF	n^+–$Al_{0.3}Ga_{0.7}As$	0.15 μm
Buffer	n^+–GaAs	0.15 μm
Substrate	n^+–GaAs substrate	

Figure 5.1. Cross section of p-$Al_xGa_{1-x}As$/p-GaAs/n-GaAs heterojunction bottom cell grown by OM-VPE.

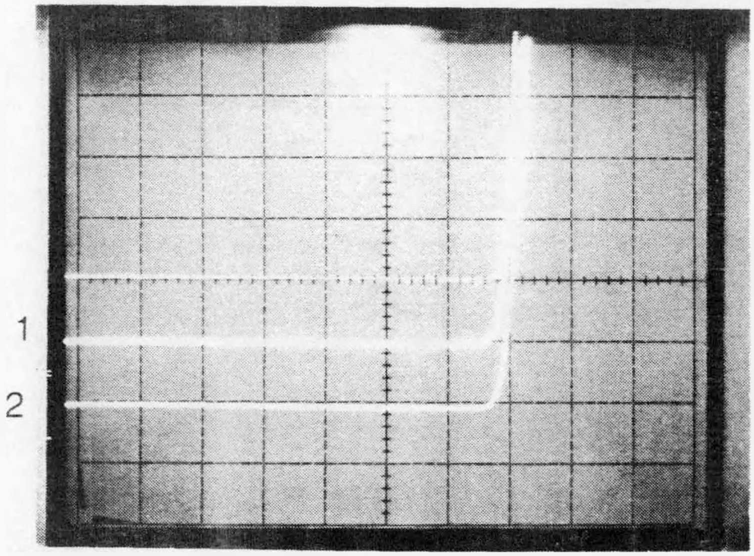

Curve 1. Vertical scale = 0.5 mA/div
Horizontal scale = 0.05 V/div

Curve 2. Vertical scale = 2 mA/div
Horizontal scale = 0.05 V/div

Figure 5.2. Illuminated and dark characteristic of p-$Al_xGa_{1-x}As$/ p-GaAs/ n-GaAs bottom cell. Curve 1 : 1 AM0 sun, curve 2 : 8 AM0 suns. (growth temperature = 650 °C)

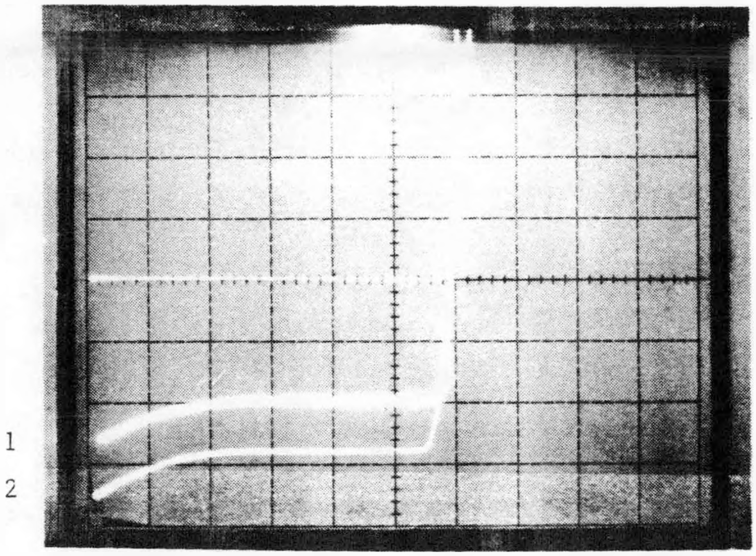

Curve 1. Vertical scale = 1.0 mA/div
Horizontal scale = 1.0 V/div

Curve 2. Vertical scale = 5 mA/div
Horizontal scale = 1.0 V/div

Figure 5.3. Illuminated and dark characteristic of p-$Al_xGa_{1-x}As$/p-GaAs/ n-GaAs bottom cell. Curve 1 : 1 AMO sun, curve 2 : 7 AMO suns. (growth temperature = 700 °C)

The present structures are limited in efficiency because of the nonoptimized layer thicknesses and dopant levels and the lack of an AR coating. The most important factor is nonoptimized hole concentration; the Mg content is graded due to the system memory effect, and as we reconfigure our system, better GaAs bottom cells are expected.

5.2 P–$Al_xGa_{1-x}As$/n–$Al_xGa_{1-x}As$ Heterojunction Top Cell Development

The basic $Al_xGa_{1-x}As$ cell structure is shown in Figure 5.4. This structure consists of a 0.5 μm-thick $Al_xGa_{1-x}As$ ($x = 0.7$) back surface field (BSF), a 3 to 5 μm-thick n-type $Al_xGa_{1-x}As$ ($x \sim 0.3$) base layer and a graded-bandgap, Mg-doped $Al_xGa_{1-x}As$ emitter in which x varies from 0.3 to ~0.7 in 0.4 μm. A 0.2 μm-thick Mg-doped $Al_xGa_{1-x}As$ ($x \sim 0.7$) layer is grown after the graded layer and is followed by a heavily p-doped GaAs cap (~0.2 μm) to facilitate contacting.

Temperatures of 700 and 750 °C have been used for the top cell growths. The results have been mixed. The surface morphologies are mirror-like and shiny to the naked eye but performance has been poor. For the 700 °C growths, the best open circuit voltage is 0.98 V (1, AM0 sun) and 1.1 V (7, AM0 suns), and the fill factors is about 0.7, as shown in Figure 5.5. Short circuit current density J_{sc} for this cell is low at 1.21 mA/cm^2. The measured external quantum efficiency (with no AR coating) is shown in Figure 5.6. For growth the 750 °C, the best open circuit voltage measured thus far is 1.04 V (1, AM0 sun) and 1.18 V (9, AM0 suns). Fill factors are about 0.64. The best

Cap	p^+GaAs		0.2 μm
Window	P–$Al_{0.7}Ga_{0.3}As$	$\chi \sim 0.7$	0.2 μm
Emitter	p–$Al_xGa_{1-x}As$	$0.3 \leq \chi \leq 0.7$	0.4 μm
Base	n–$Al_xGa_{1-x}As$	$\chi \sim 0.3$	$3 \sim 5$ μm
BSF	n^+–$Al_xGa_{1-x}As$	$\chi \sim 0.7$	0.5 μm
Substrate	n^+–GaAs substrate		

Figure 5.4. Cross section of $Al_xGa_{1-x}As$ top cell structure grown by OM-VPE.

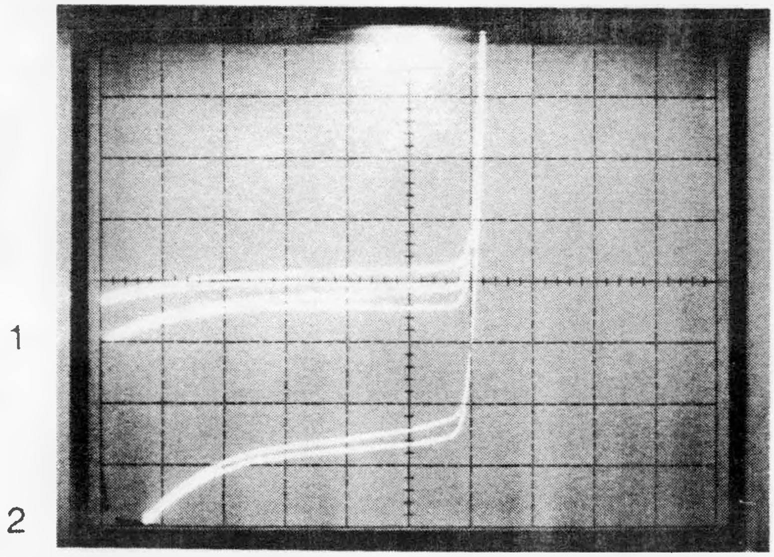

Vertical scale = 0.5 mA/div
Horizontal scale = 1.0 V/div

Figure 5.5 Illuminated and dark characteristic of $Al_xGa_{1-x}As$ heterojunction top cell. Curve 1 : 1 AMO sun, curve 2 : 7 AMO suns. (growth temperature - 700 °C)

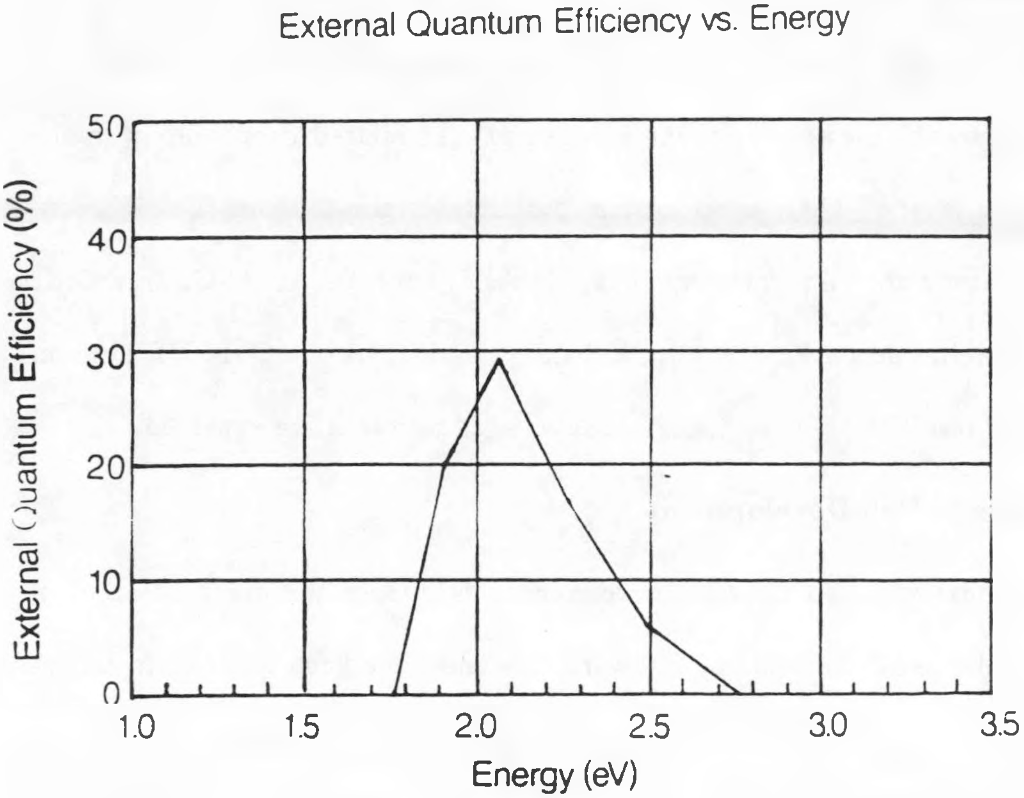

Figure 5.6. External quantum efficiency of $Al_xGa_{1-x}As$ top cell without AR coating. Energy gap ≈ 1.8 eV.

I-V characteristic is shown in Figure 5.7. J_{sc} (1 sun) is also low at about 1.45 mA/cm^2. No improvement of the external efficiency has been correlated to the higher growth temperature.

The main reason for the poor $Al_xGa_{1-x}As$ cell performance is believed to be related to the growth temperatures and oxygen-related deep centers in the $Al_xGa_{1-x}As$ layers. These deep centers probably originate from the high content of water vapor and/or oxygen in the AsH_3 source. An Al-Ga-In eutetic bubbler for in-line AsH_3 scrubbing is being installed in our OM-VPE system, and better results for low temperature $Al_xGa_{1-x}As$ growth are expected.

5.3 Cascade Cell Development

The next stage in Ge IOC development is clearly the demonstration of cascade solar cells. Several steps toward this end have been taken. An unambiguous demonstration of voltage addition in the cascade cells has been achieved this year. In this section, we present the results and address the limiting factors for a high-efficiency performance.

5.3.1 Cascade Cell Processing

The processes of multilayer cascade solar cells have been presented in detail in the last annual report. Difficulties of patterning tunnel junctions have also been described earlier in Section 4.3.

For making ohmic contacts to n$^+$-GaAs substates, 300 Å of Sn followed by 3000 A of Ag is evaporated onto the device. These are large area contacts and produce reproducible ohmic behavior after alloying at 450 °C for 1

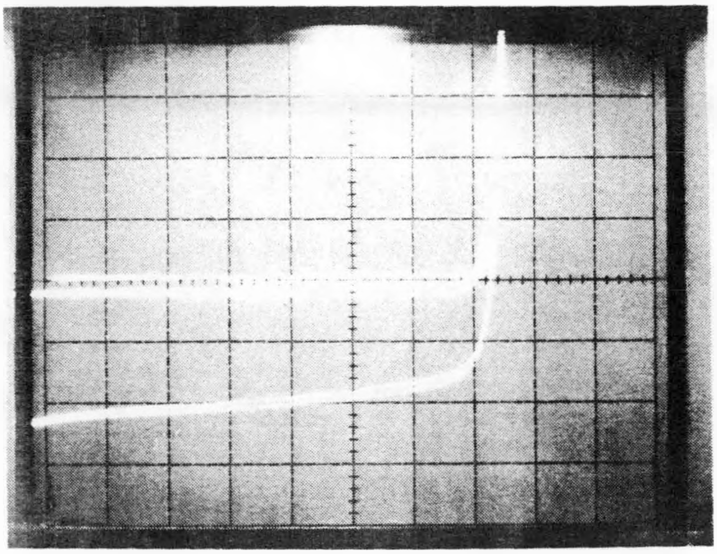

Horizontal: 0.5 V/div
Vertical: 0.2 mA/div

Figure 5.7. Illuminated and dark characteristic of $Al_xGa_{1-x}As$ heterojunction top cell -
1 sun: Jsc = 1.45 mA/cm^2, V_{oc} = 1.04 V;
9 suns: Jsc = 13.1 mA/cm^2, V_{oc} = 1.18V.

minute. For making ohmic contacts to front p^+-GaAs layers, 100 Å of Mn followed by 900 Å of Au are evaporated. No Au electroplating was used to thicken these contacts.

5.3.2 Cascade Cell Performance

During the final quarter of this program, we have fabricated cascade cells composed of a AlGaAs top cell (growth temperature = 700°C) and a GaAs bottom cell (growth temperature = 650 °C). The I-V characteristic for the best cell is shown in Figure 5.8. Open circuit voltages are 1.26 and 1.44 volts at 1 and 7 suns, respectively. These open circuit voltages are greater than any single-junction values measured in our laboratory and indicate a voltage addition of the two junctions. Further evidence of the achievement of a cascade cell is the double breakdown characteristic shown in this figure. Under illumination and reverse bias, two levels of reverse current saturation are seen. The two levels of current indicate the short circuit current values of the two cells. For low reverse voltages, the current is limited by the smallest of the photocurrents from the AlGaAs top cell. When breakdown occurs in the AlGaAs top cell at about 2 volts, the reverse current then becomes limited by the photocurrent from the GaAs bottom cell. Finally, at larger voltages, around 5 volts, reverse breakdown of the GaAs occurs. In this cell, J_{sc} is low, about 2.2 mA/cm^2 at 7 suns, and the fill factor is poor, about 0.45 at both 1 and 7 suns. The main performance limitations causing the low J_{sc} originate in the AlGaAs junction. The spectral response shown in Figure 5.9 indicates collection from both junctions. The quantum efficiency, however, is very poor.

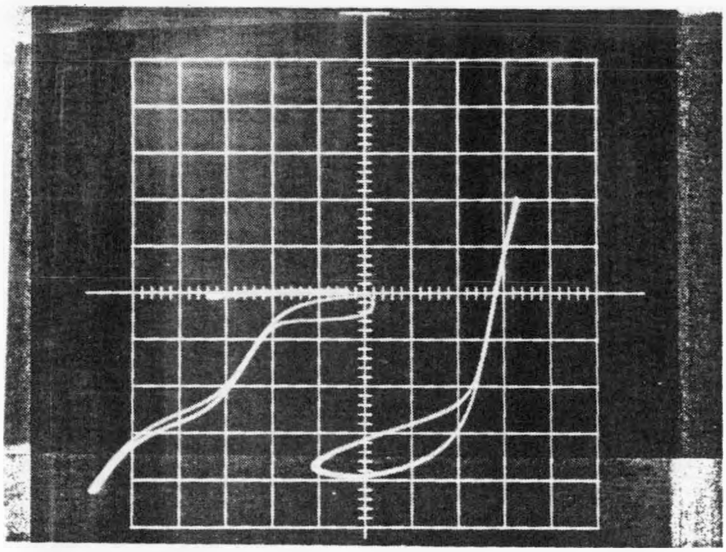

Forward: 0.5V/div
0.1 mA/div

Reverse: 1.0 V/div
1.0 mA/div

Figure 5.8. Dark and illuminated I-V characteristics for patterned cascade cell at 7 suns : Jsc = 2.2 mA/cm^2, V_{oc} = 1.44 V.

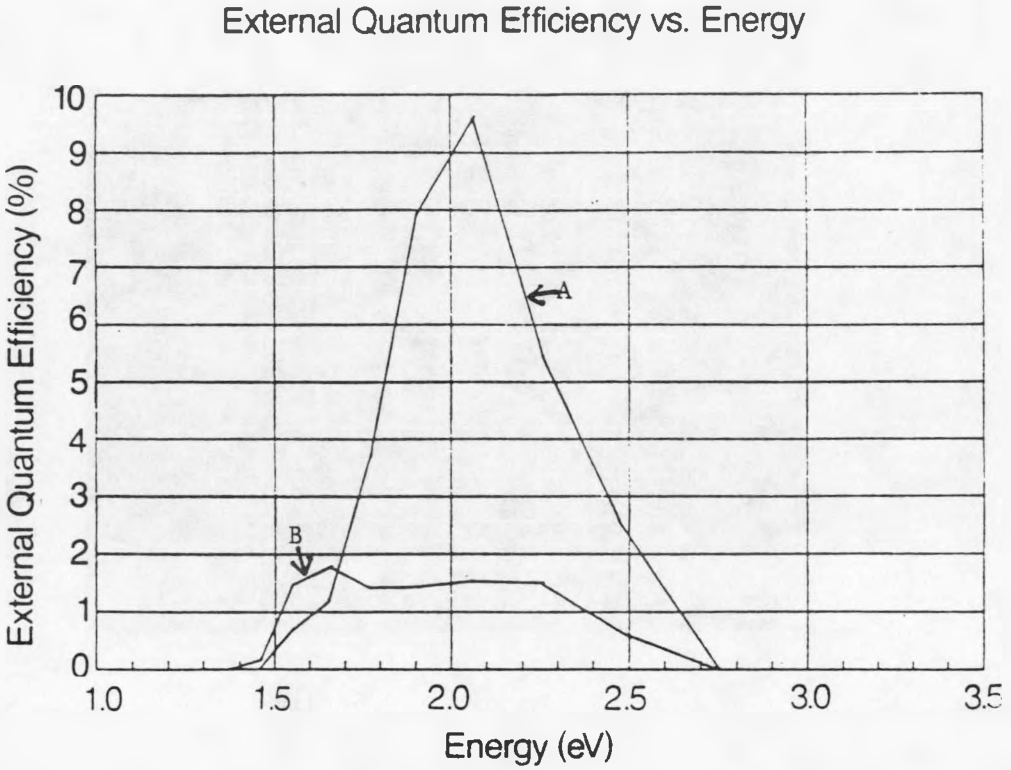

Figure 5.9 Measured external quantum efficiency for cascade cell structure: curve A measured with red bias filter; curve B measured with green bias filters. No AR coating on sample.

especially at the bottom junction. Because of undercutting, some Ge was intentionally left on the surface, and the optical loss in the Ge layer is partly responsible for the poor efficiency at the bottom junction.

Cascade cells using AlGaAs grown at 750 °C have also been fabricated. I-V characteristic for the best cell is shown in Figure 5.10. The double-breakdown is present at the reverse bias under illumination although both junctions are leaky. The J_{sc} value, around 13.7 mA/cm^2 at 7 suns, is slightly improved over the cell grown at 700 °C. Growth at 750 °C resulted in a degradation of the cell. Voltage (0.8 V at 1 AM0 sun. and 1.1 V at 7 AM0 suns) is poor although the spectral response, shown in Figure 5.11, clearly indicates collections from both junctions. For the bottom cell, quantum efficiency is greater when compared to the quantum efficiency of the bottom cell shown in Figure 5.9, probably the result of complete removal of the Ge between the fingers of the IOC.

To summarize the results, cells showing unambiguous cascade action have been grown. AlGaAs junctions, grown at low temperature without moisture scrubbing on gas lines, limit device performance. For Ge patterning, a better etching technique is needed. As these problems are solved. the cascade structure may well fulfill the modeled predictions for high efficiencies.

5.4 Fabrication of Triangular Top Contact

The triangular contact can minimize the obscuration and can enhance both the short-circuit current and open-circuit voltage, improving cell

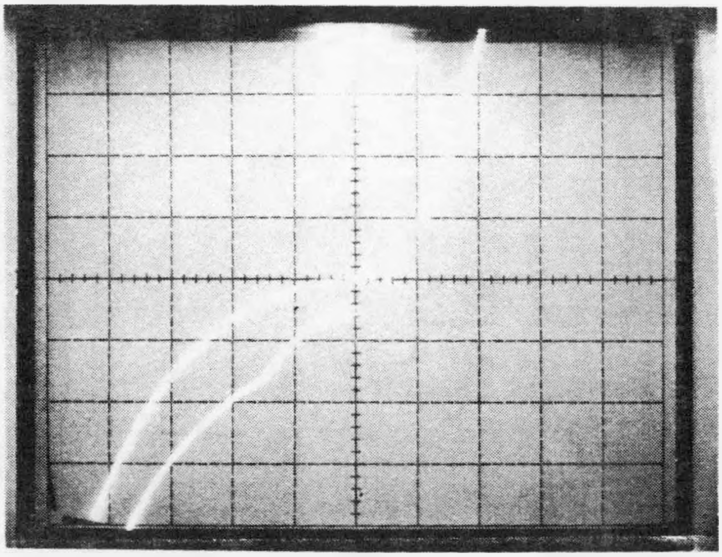

Horizontal = 2 V/div
Vertical = 5 mA/div

Figure 5.10. Illuminated and dark characteristics for patterned cascade cell at 7 suns : Jsc = 13.7 mA/cm^2, V_{oc} = 1.1 V.

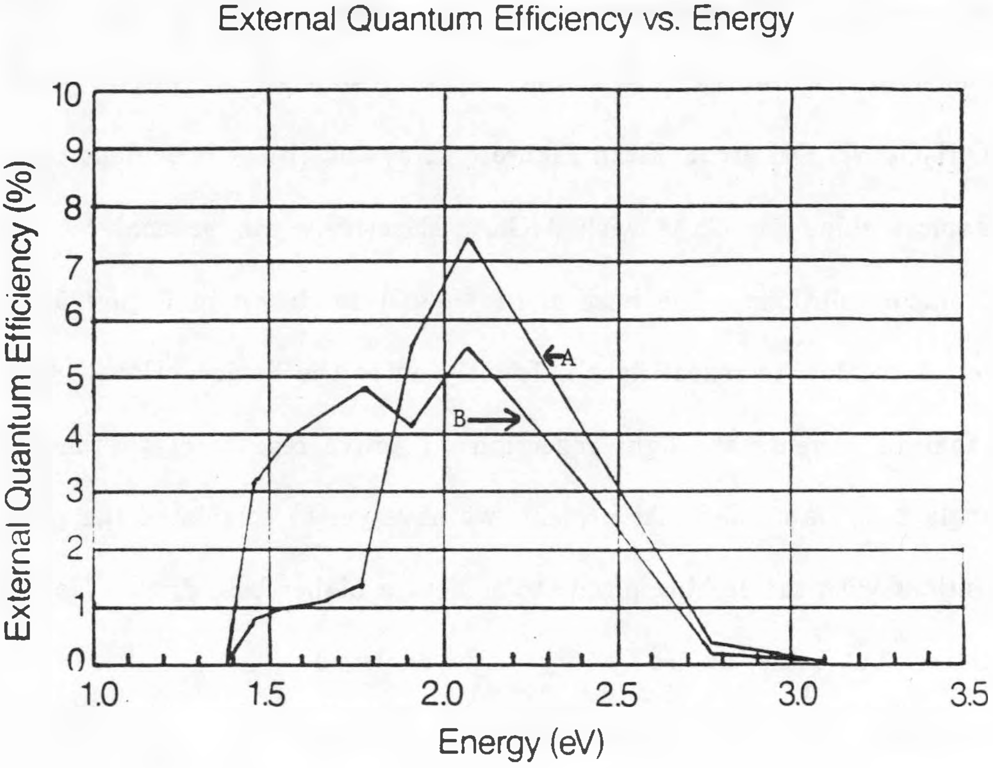

Figure 5.11. Measured external quantum efficiency for cascade cell structure: curve A measured with red bias filter; curve B measured with green bias filters. No AR coating on sample.

efficiency. To develop this triangular contact, wet chemical etching has been initially evaluated. H_2O-H_2O_2-NH_4OH solutions are prime candidates since these etchants are frequently used to etch GaAs selectively on AlGaAs stop etch layers. After samples are etched, cross-sectional micrographs are examined which represent portions of cleaves through both of the different orthogonal cleavage directions ([011] and [011]) lying in the (100) plane. Figure 5.12(a) shows the (011) cross-sectional profile after a $20H_2O$:$20H_2O_2$:NH_4OH etch, whereas Figure 5.12(b) is the (011) cross-sectional profile after a 10 H_2O:H_2O_2 NH_4OH etch. From Figure 5.12(a) and (b), it is evident that an anisotropic etching for GaAs with AlGaAs selectively can be achieved using wet chemical solutions. The base angle (~30°) as shown in Figure 5.12(b), however, is too low to reflect light efficiently on to the device. Hovel [8] indicated that to increase the light reflection on active regions of the device, a base angle $>45°$ is needed. At present, we have yet to correlated the etchant compositions with the etching profile to achieve a higher base angle. However, we believed that higher angles (~55°) can be achieved.

To summarize, the H_2O-H_2O_2-NH_4OH etchants may be suitable for developing triangle contact although higher base angles ($\geq 45°$) have yet to be achieved. One alternative is using a dry reactive-ion etch process of CCl_2F_2 and He. This process can be adjusted to obtain a more optimum GaAs structure of triangle cross section with ~75° base angles [9].

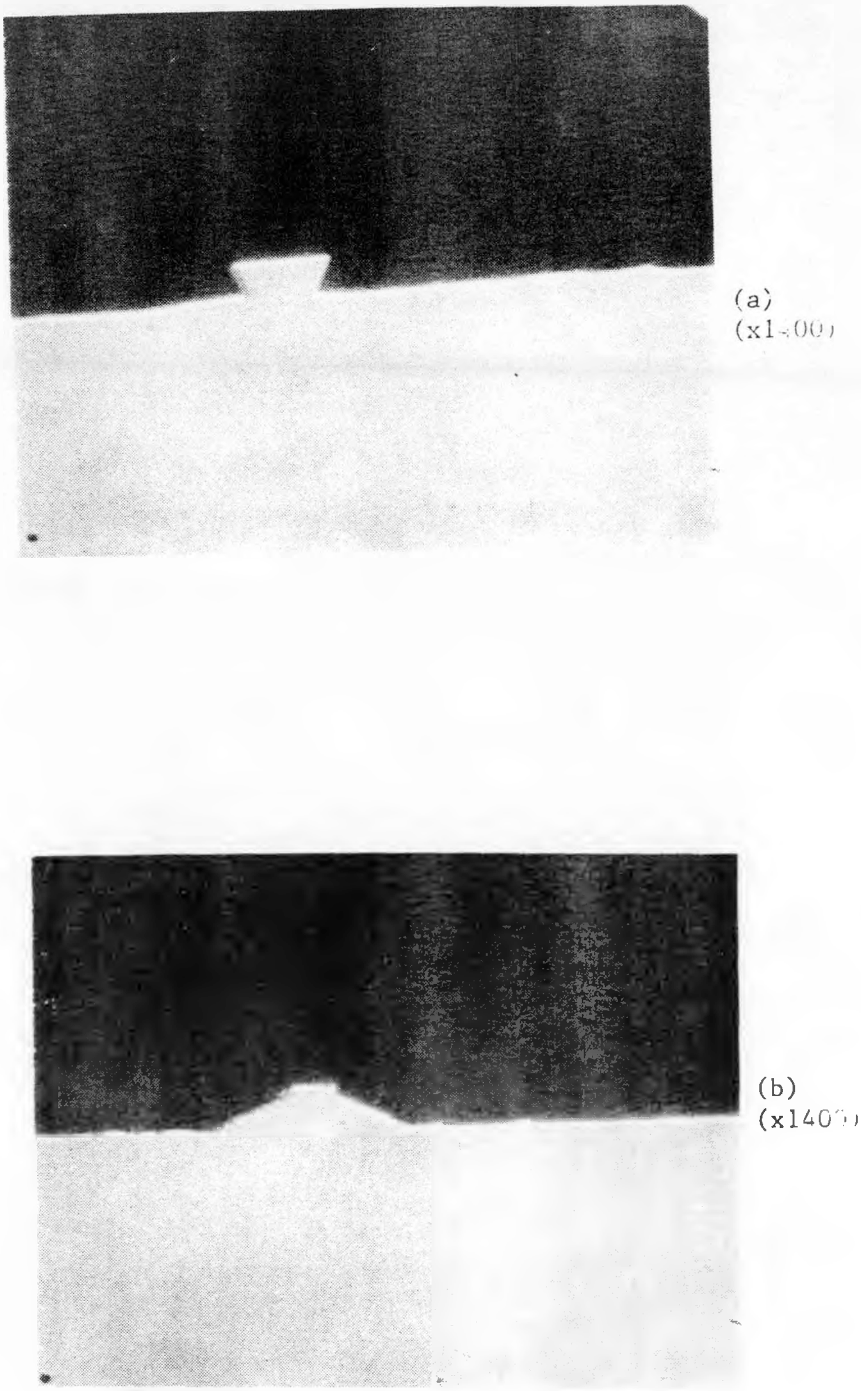

Figure 5.12. (a) (011) GaAs cross-sectional profile after a 20 H_2O:20 H_2O_2: NH_4OH, and (b) (01$\bar{1}$) GaAs cross-sectional profile after a 10 H_2O:H_2O_2:NH_4OH etch.

6.0 RECOMMENDATIONS FOR FUTURE RESEARCH

Based on our experience, recommendations which are thought to be valuable for further research are suggested below:

(1) The dopant control problem using Cp_2Mg or MCpMg should be corrected with a vent/run configuration. In a system using the vent/run configuration, the Mg line can be equilibrated before the Mg reactants are switched into the reactor. Thus, the "memory effect" problem is eliminated. Once this problem is solved, a more controllable p-type dopant for GaAs and $Al_xGa_{1-x}As$, and thus a more abrupt p-n junction, can be achieved.

(2) The major factor for the poor $Al_xGa_{1-x}As$ cell performance is believed to be related to the growth temperatures and oxygen-related deep centers in the $Al_xGa_{1-x}As$ layers. These deep centers probably originate from the high content of water vapor and/or oxygen in the AsH_3 source. In-line AsH_3 scrubbing is suggested. Better low temperature $Al_xGa_{1-x}As$ growth will likely result.

(3) Due to the difficulty of patterning Ge intercell ohmic connections. a selective epitaxy for n^+-GaAs/p^+-Ge/p^+-GaAs is suggested. This can be done by the plasma deposition of Si_3N_4 and then photolithographically defining the IOC pattern. After the Si_3N_4 film pattern is defined, samples can be loaded in III-V reactor to grow a sandwiched structure of n^+-GaAs/p^+-Ge/p^+-GaAs. After growth, the sample is removed

from the reactor and dipped in a buffered HF solution to lift off unwanted material, leaving the patterned IOC.

(4) To develop a triangular top contact, a dry reactive-ion etch process of CCl_2F_2 and He [9] is suggested. This process can be adjusted to obtain a more optimum base angle, possibly reaching 75° to achieve a more efficient light absorption.

If all of the above technology improvements are implemented, performance of the first patterned cascade cell will likely improve dramatically.

7.0 REFERENCES

1. D. L. Miller, S. W. Zeas, and J. S. Harris, Jr., J. Appl. Phys.. 53. 744 (1982).
2. R. Azoulay, L. Dugrand, D. Ankri, and E. V. K. Rao, J. Cryst. Growth. 68, 453 (1984).
3. C. R. Lewis, W. T. Dietze, and M. J. Ludowise, J. Electron. Mater.. 12. 507 (1983).
4. A. W. Nelson and L. D. Westbrook, J. Cryst. Growth, 68, 102 (1984).
5. S. M. Sze, Physics of Semiconductor Devices, John Wiley and Sons. New York, p. 5 (1969).
6. M. L. Timmons, Annual Technical Progress Report, prepared for the Solar Energy Research Institute under Subcontract No. XL-4-03032-6, 1984.
7. G. L. Kuhn and C. J. Rhee, J. Electrochem. Soc., 120, 1563 (1973).
8. H. J. Hovel, Solar Cells, in Semiconductors and Semimetals, Vol. II. Academic Press, New York (1975).
9. K. Hikosaka, T. Mimura, and K. Joshin, Japan. J. Appl. Phys., 20, L847 (1981).